University of Twente

EEMCS / Electrical Engineering
Control Engineering

Flexible Needle Steering using a Mechanics-Based Approach

Roy Roesthuis

MSc report

Supervisors
Prof. dr. ir. S. Stramigioli
Dr. S. Misra
Prof. dr. ir. H.F.J.M. Koopman
M. Abayazid, MSc

November 2011

Report nr. 021CE2011
Control Engineering
EE-Math-CS
University of Twente
P.O. Box 217
7500 AE Enschede
The Netherlands

Abstract

Flexible needles with asymmetric needle tips naturally deflect when inserted into soft tissue due to an asymmetric distribution of forces at the needle tip. By rotating the needle during insertion, the direction of deflection is changed and this enables needle steering. To accurately steer a needle towards a desired location inside a tissue, knowledge is required about needle deflection. This study focusses on developing a model which predicts deflection of flexible needles with asymmetric (bevel) tips using a mechanics-based approach.

In the first part of the study, the mechanics of needle-tissue interactions are investigated. Needle tip and friction forces are identified by performing needle insertion experiments. Steel needles with a bevel tip are used for the experiments and gelatin phantom is used as a soft tissue simulant. The tip force is used in a mechanics-based model to predict needle deflection for a needle having a single bend. It was shown that for this single bend case, needle deflection could be simulated with an average error of 0.2 mm.

In the second part of the study, the proposed model presented in the first part is modified to predict needle deflection for a needle having multiple bends. In this study, flexible Nitinol needles with bevel tips are used for experiments. These Nitinol needles are more flexible than steel needles, resulting in more deflection when inserted into a soft tissue. A distributed load which acts along the needle shaft is introduced and evaluated by fitting the model to experimental results. Using this load in the mechanics-based model, it is shown that final needle tip deflection can be predicted for the double bend case with a targeting error of 1.1 mm.

In third and last part, the mechanics-based model is used to steer a 0.8 mm diameter Nitinol needle towards a desired target location. The mechanics-based model is used as a pre-operative planner to determine when needle rotation needs to be performed. Two cases of needle steering are evaluated. In the first case experiments are performed in which there is no image feedback. Rotation is performed at the location as determined by the mechanics-based model. This resulted in a maximal targeting error of 0.5 mm with a standard deviation of 0.5 mm. Results were compared when a kinematics-based bicycle model is used to determine the rotation for needle rotation, and targeting error was found to be equal. The maximum observed error was found to be reduced: 1.1 mm using the bicycle model and 0.6 mm for the mechanics-based model. In the second case, image feedback of needle tip position is used to control needle rotation during insertion. By using image feedback, it is shown that variations in needle tip deflection can be taken into account. Maximal targeting error using image feedback was 0.6 mm and did not reduce due to a systematic error in the control algorithm, standard deviation was reduced to 0.1 mm.

Acknowledgements

This project would not have been possible without the help of a number of people. First of all I would like to thank my supervisor Dr. Sarthak Misra, who accepted me into working on this project and gives me the possibility to continue working in the interesting area of medical robotics as a Phd student. I would also like to thank Dr. Jorn op den Buijs, who was of great advice in the beginning of the project, but he unfortunately decided to leave for a different job. Momen Abayazid joined the group halfway into the project, but despite that fact he has been of great help and always made time for me.

During the project the CE technicians have been of great help. I would especially like to thank Alfred de Vries for making the containers for the gelatine phantoms and Gerben te Riet o/g Scholten for thinking about ways to polish bevel tips on the needles. The CE secretary has also been of support when I needed them, especially at the end of the project: so thanks for the help Carla and Jolanda!

During this project I have found that it is not just the challenges in the project that kept me motivated. The regular group we took breaks with is something which I truly appreciated. The often hilarious discussion we had during these meetings would get my thoughts out of the project for a minute; something I believe is important to keep you motivated. So thanks for the interesting group of people I had the chance of having breaks with!

Last but not least I would like to thank my family in supporting me, especially my parents Jan and Henriëtte. I know that I have not always kept them updated about what I was doing and I might have been out cycling all day for as far they knew. So thanks for keeping faith in me!

— Roy Roesthuis

Contents

Introduction

The last decade there has been an increasing interest in research into Minimally Invasive Surgery (MIS). Laproscopic surgery is an example of MIS. In laporoscopic surgery, instruments are introduced in the abdomen through small incisions (0.5 - 1.5 cm). Traditional open surgery requires much larger incisions (∼20 cm). Due to the smaller incisions, MIS has several advantages over traditional open surgery. These include reduced pain for the patient, shorter recovery time and smaller scars.

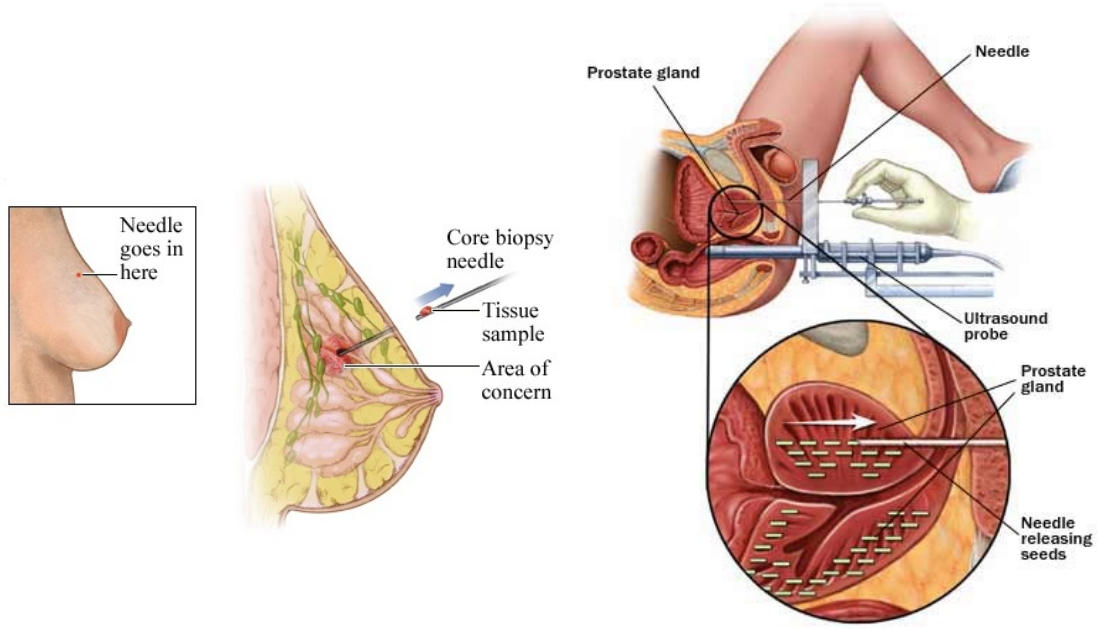

(a) (b)

Figure 1: Examples of procedures in which needles are used to reach a certain location in the human body. (a) Breast biopsy: the needle is used to take a tissue sample for diagnosis (© Healthwise, Incorporated). (b) Brachytherapy: a needle is used to place radioactive seeds near a tumor for treatment (© Mayo Foundation for Medical Education and Research).

Needles can be used in some medical procedures as opposed to open surgery. Open surgery is a lot more stressful for the patient and there is a risk of complications during the procedure. Needles are used for biopsy procedures, in which the needle is used to take a tissue sample for diagnosis. In Fig. 1a, a needle is used in a breast biopsy to diagnose for cancer. Needles can also be used to perform localized treatment of malignant tissue. Fig. 1b shows a brachytherapy procedure in the prostate, in which a needle is used to place radioactive seeds near a tumor. Using a needle minimizes partient discomfort, but may lead to an inconclusive diagnosis in the case of a biospy procedure due to targeting errors. Hypodermic needles used in these procedures have asymmetric (bevel) tips which causes them to deflect during insertion, making it challenging to reach the lesion within the breast. Also tissue inhomogeneity and other physiological processes can cause the needle to deflect differently than expected. This can result in a misdiagnosis when the

needle tip is misplaced. Imaging modalities such as ultrasound can assist the physician in reaching the lesion. Manually steering a needle towards a desired location requires a lot of experience and dexterity. Even then the physician may still miss the target and multiple insertions are required, increasing patient discomfort.

Using a robotic system to steer the needle can improve needle placement and can reduce the time it takes to perform the procedure. The robotic system uses knowledge about how the needle will deflect depending on needle and tissue properties to accurately steer the needle. Medical imaging modalities such as MRI or ultrasound can provide the system with information about needle tip position, enabling intra-operative control of the needle.

Decreasing needle diameter increases needle flexibility. Flexible needles allow more curved needle paths and this can be used to steer the needle around sensitive anatomical obstacles such as blood vessels or nerves (Fig.2). Thinner needles result in less damage of the tissue as opposed to the traditional, thicker needles used in these procedures.

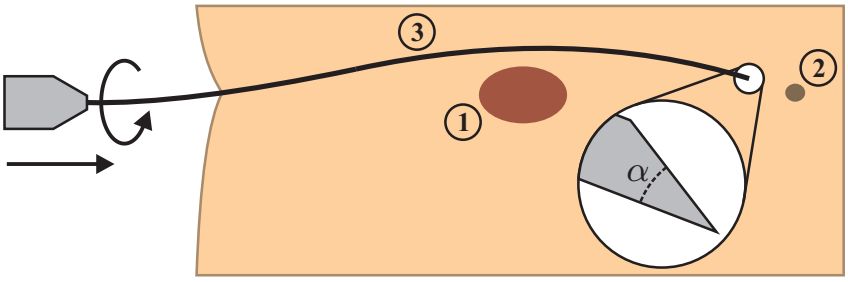

Figure 2: Schematic drawing showing the concept of steering a flexible needle. Flexible needles with asymmetric (bevel) tips ③ naturally bend when inserted into soft tissue. This can be used to steer the needle around an obstacle ① towards a target ②.

Thesis Outline

This thesis is composed of three manuscripts: In the first manuscript, the mechanics of needle-tissue interaction are investigated and used to derive a mechanics-based model to simulate needle deflection for the single bend case. The second manuscript extends on the first manuscript by modifying the mechanics-based model such that needle deflection can be predicted for a needle having multiple multiple bends. Finally, the third manuscript uses the mechanics-based model to steer the needle towards a desired target location. The thesis is concluded by reflecting on the work done and providing directions and recommendations for future work.

Thesis Contributions

[1] R.J. Roesthuis, Y.R. Van Veen, A. Jahya and S. Misra, "Mechanics of Needle-Tissue Interaction," *Proceedings of IEEE International Conference on Intelligent Robots and Systems (IROS)*, San Francisco, USA, pp. 2557-2563, Sep-Oct 2011.

[2] R.J. Roesthuis, M. Abayazid and S. Misra, "Mechanics-Based Model for Steering Flexible Needles," *Proceedings of the IEEE International Conference on Robotics and Automation (ICRA)*, St. Paul, USA, May 2012, Under Review.

[3] R.J. Roesthuis, M. Abayazid and S. Misra, "Steering of Flexible Needles with a Bevel Tip," *Proceedings of the Fourth IEEE International Conference on Biomedical Robotics and Biomechatronics (BioRob)*, Rome, Italy, June 2012, In Preparation.

Part I

‘Mechanics of Needle-Tissue Interaction’

Mechanics of Needle-Tissue Interaction

Roy J. Roesthuis, Youri R.J. van Veen, Alex Jahya and Sarthak Misra
MIRA - Institute of Biomedical Technology and Technical Medicine, University of Twente, The Netherlands

***Abstract*— When a needle is inserted into soft tissue, interaction forces are developed at the needle tip and along the needle shaft. The needle tip force is due to cutting of the tissue, and the force along the needle shaft is due to friction between needle and tissue. In this study, the friction force is determined for needles inserted into a gelatine phantom at insertion velocities of 10 mm/s and 20 mm/s. The friction force is found to be dependent on the insertion velocity. The needle tip force is calculated using the friction and insertion force, and is used as input for a mechanics-based model which predicts the amount of needle deflection. In the model, the needle is considered to be a cantilever beam supported by springs which have needle-tissue interaction stiffness (K_e). The value of the interaction stiffness is evaluated by comparing results from experiments and simulation. A mechanical needle insertion device is used to insert needles. Needle deflection during insertion is determined using a needle tip tracking algorithm. Results of this study provide insight into the mechanics of needle-tissue interaction, and can be used in studies for robotically steering needles into soft tissue.**

I. Introduction

Percutaneous needle insertion is one of the most common minimally invasive medical procedures that is performed for local drug delivery, brachytherapy and biopsy. Accurate needle placement in these procedures is of importance, mainly because biopsy of an unintended tissue region can result in misdiagnosis, or in case of brachytherapy, malignant tissue is not destroyed. Inaccuracy of needle placement can be caused by several factors such as tissue inhomogeneity, tissue anisotropy, anatomical obstructions during needle insertion, and physiological processes like fluid flow and respiration.

Targeting accuracy in percutaneous needle insertion procedures can be improved by using a robot to insert needles. A number of research groups have studied the concept of robotic needle insertion [1]–[8]. Some of these groups have studied the use of thin bevel-tipped needles for needle insertion [1], [3], [4], [8]–[11]. The advantage of using thin needles with bevel tips is that they naturally bend during insertion due to assymetric distribution of forces at the needle tip (Fig. 1). This needle bending can be used to steer a needle through soft tissue. To be able to do pre-operative path planning and accurately steer a bevel-tipped needle using a robot, a model is required which predicts the amount of needle deflection during insertion into soft tissue [4].

In this study a mechanics-based model, based on the work by Misra et al. [4], is presented which predicts the amount of needle deflection. Though an analytical mechanics-based model is less complex than a finite element-based approach, it provides greater insight and framework for modeling needle-tissue interactions. The mechanics-based model requires knowledge about needle-tissue interaction forces (Fig. 1). The force along the needle shaft (F_f) is due to friction between needle and tissue, and the force at the needle tip (F_t) is a result of cutting of the tissue during insertion. Several studies have been performed to investigate the forces acting on the needle during insertion into soft tissue. Kataoka et al. [12] inserted a needle with a triangular pyramid tip into a canine prostate while measuring the insertion force. By using a needle consisting of an outer and inner part, they were able to extract the tip and the frictional force along the needle shaft from the insertion force. Okamura et al. [13] also succeeded in identifying frictional and tip forces from the insertion force measured at the base of the needle. In their experiments, needles with various bevel angles and diameters were inserted into bovine liver. They assumed that the forces at the needle tip were constant for a given tissue (i.e. independent of the internal tissue stiffness). However, their experimental result showed that the tip force increased proportionally with insertion depth due to increasing occurrences of needle collisions with internal structures in the tissue. Misra et al. [14] improved on this study by considering that the force acting on the needle tip was dependent on tissue stiffness. The goal of this work is to identify the needle-tissue interaction forces and predict needle deflection using the mechanics-based model.

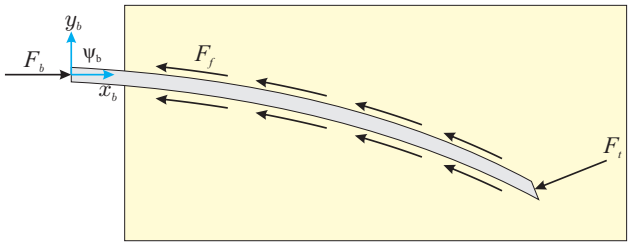

Fig. 1. As a bevel-tipped needle is inserted into a soft tissue, interaction forces are developed: F_b is the insertion force measured at the needle base, F_f is the friction force along the needle shaft and F_t is the force at the needle tip due to cutting of the tissue. The coordinate frame located at the base of the needle is indicated by ψ_b.

The paper is organized as follows: Section II describes the needle-tissue interaction forces during insertion. In Section III, a mechanics-based model which predicts the amount of needle deflection for a bevel-tipped needle inserted into a soft tissue is derived. Section IV describes the setup used to record the forces during insertion into a gelatine phantom. It also describes the tracking algorithm used to measure the amount of needle deflection. Section V discusses the results obtained from experiments and simulation. Finally, Section VI provides conclusions and possible directions for future work.

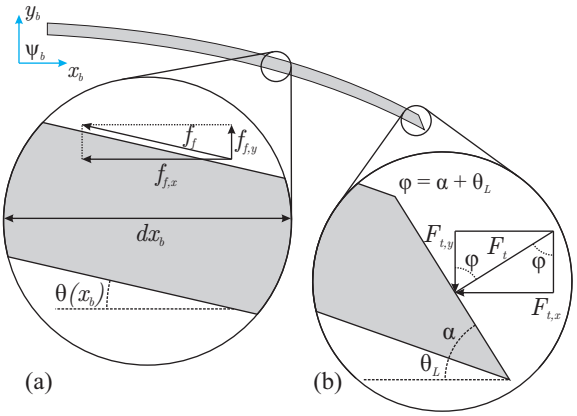

Fig. 2. Friction force along needle shaft and force at the needle tip (F_t) during insertion. (a) F_t acts normal to the needle bevel edge, $F_{t,x}$ and $F_{t,y}$ are the x_b- and y_b- component of F_t expressed in the global coordinate frame, ψ_b. $F_{t,x}$ and $F_{t,y}$ vary during insertion due to the deflection of the needle. (b) The friction force (f_f) per unit length (dx_b) along the needle shaft during insertion is decomposed to its horizontal ($f_{f,x}$) and vertical ($f_{f,y}$) components. The slope of the needle ($\theta(x_b)$) varies along the length of the needle.

II. Needle-Tissue Interaction Forces

Interaction forces are developed as a bevel-tipped needle is inserted into a soft tissue (Fig.1). These interaction forces are decomposed of a friction force along the needle shaft (F_f) and a force acting normal to the needle's bevel tip (F_t). The soft tissue is considered to be viscoelastic, this means that the friction force increases as the relative velocity between needle and surrounding tissue increases. The tip force is considered to be a result from cutting of the tissue at the needle tip [13], [14].

Due to bending of the needle during insertion into a soft tissue (Fig. 2), both the friction force and tip force are composed of components acting in the x_b- and y_b-direction (expressed in ψ_b). The needle slope ($\theta(x_b)$) is defined as the angle between the needle's centre axis and the coordinate frame at the needle's base (ψ_b) observed at location x_b along the needle shaft. Using the needle slope, the components ($f_{f,x}$ and $f_{f,y}$) of the friction force (f_f) can be evaluated

$$\begin{aligned} f_{f,x} &= f_f \cos\left(\theta(x_b)\right) \\ f_{f,y} &= f_f \sin\left(\theta(x_b)\right) \end{aligned} \tag{1}$$

where the friction force (f_f) is defined as friction per unit inserted needle length (dx_b). Total friction force in x_b- and y_b-direction ($F_{f,x}$ and $F_{f,y}$) is obtained by integrating (1) over the inserted needle length (l)

$$\begin{aligned} F_{f,x} &= \int_{L-l}^{L} f_f \cos\left(\theta(x_b)\right) dx_b \\ F_{f,y} &= \int_{L-l}^{L} f_f \sin\left(\theta(x_b)\right) dx_b \end{aligned} \tag{2}$$

where L is the total needle length (Fig. 3).

Using the slope at the needle tip ($\theta_L = \theta(L)$) and the needle's bevel angle (α), F_t can be decomposed into two components ($F_{t,x}$ and $F_{t,y}$ in Fig. 2)

$$\begin{aligned} F_{t,x} &= F_t \sin(\alpha + \theta_L) \\ F_{t,y} &= F_t \cos(\alpha + \theta_L) \end{aligned} \tag{3}$$

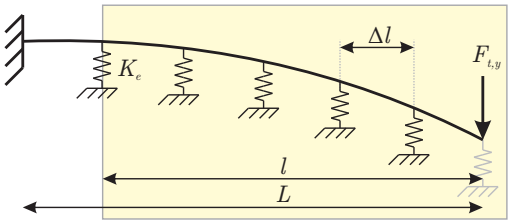

Fig. 3. The tissue elastically supports the needle as it is inserted into the tissue. This is modeled as a cantilever beam supported by a series of springs (with effective stiffness K_e) along the needle shaft and $F_{t,y}$ as the transverse tip force. The total needle length is L and the inserted needle length is l.

The insertion force (F_b) is the force required to insert a needle into a tissue (Fig. 1). At a given instant in time during insertion, the forces along the x_b-axis are in equilibrium and can be expressed as

$$F_b = -(F_{t,x} + F_{f,x}) \tag{4}$$

If the amount of friction during needle insertion is known, the needle tip force ($F_{t,x}$) can be calculated by subtracting the friction force ($F_{f,x}$) from the insertion force (F_b). Using (3) and the horizontal tip force ($F_{t,x}$), the transversal tip force ($F_{t,y}$) can be calculated. This force is used as input for a mechanics-based model which is presented in the next section.

III. Mechanics-Based Model

In this section, a mechanics-based model is developed which predicts the deflection of a bevel-tipped needle during insertion into soft tissue. In the proposed model, this is modeled as a cantilever beam supported by a series of springs which each have interaction stiffness, K_e (Fig. 3). The interaction stiffness of these springs is considered to be constant throughout the tissue. Transversal tip force ($F_{t,y}$) is taken as input and causes the needle to deflect in transversal direction. The needle will also compress in the axial direction due to $F_{t,x}$, but due to high stiffness of the needle in the axial direction this deflection is very small compared to transversal bending and is therefore neglected. The Rayleigh-Ritz method is used to evaluate the needle deflection during insertion. This method will be described in more detail in Section III-A.

The modeling of inserting a bevel-tipped needle into tissue is discretized into a series of insertion steps (Fig. 4). Each insertion step is denoted by i and the total number of insertion steps is n. In each step, the inserted needle length (l_i) is increased by Δl and the additional deflection due to transversal tip force ($F_{t,y}$) is calculated:

- Insertion step i, sub-step 1: Initially the needle is a distance l_i inside the tissue and is modeled as a cantilever beam supported by springs (configuration ⓐ) which each have stiffness K_e. In this step, transversal tip force $F^i_{t,y}$ is calculated using (3).
- Insertion step i, sub-step 2: Transversal tip force ($F^i_{t,y}$), calculated in sub-step 1, is applied and the amount of needle deflection is determined using the Rayleigh-Ritz method based on the cantilever beam model in

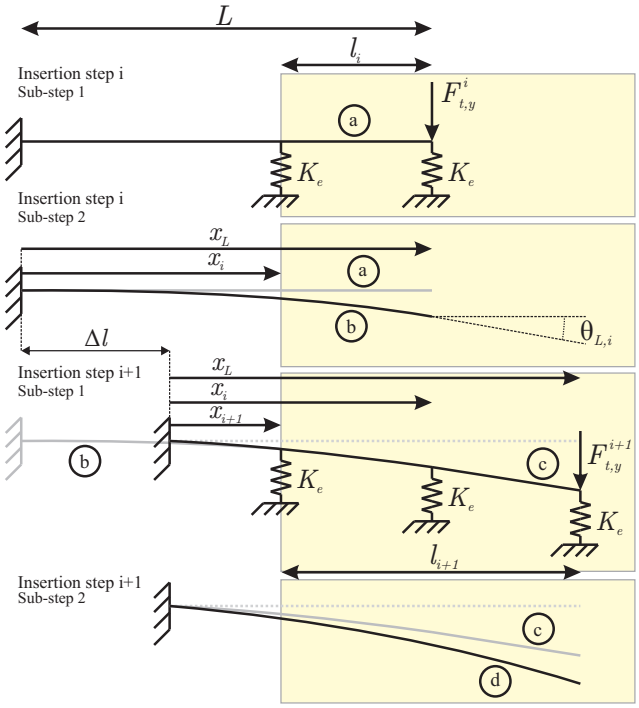

Fig. 4. Needle insertion into a tissue is modeled in a series of insertion steps. Each insertion step (i) is divided into 2 sub-steps: in the first sub-step the inserted needle distance is increased with Δl and a spring of stiffness K_e is added. In the second sub-step, the deflected needle shape is calculated by applying transversal tip force $F_{t,y}$.

sub-step 1. This results in the needle to deflect to configuration ⓑ and tip slope $\theta_{L,i}$ is calculated.

- Insertion step $i+1$, sub-step 1: Starting with configuration ⓑ, the inserted needle length is further increased with a distance Δl and this results in configuration ⓒ. An additional spring is added and tip force $F^{i+1}_{t,y}$ is calculated using (3).
- Insertion step $i+1$, sub-step 2: Transversal tip force $F^{i+1}_{t,y}$ is applied and the needle deflects to configuration ⓓ using similar steps described in sub-step 2 of step i.

The process of needle insertion continues until the final inserted needle length (l_n) is reached. The increase in inserted needle length (Δl) at each step of insertion is determined by the final inserted needle length (l_n) and the number of insertion steps (n): $\Delta l = l_n/n$.

A. Rayleigh-Ritz Method

The Rayleigh-Ritz method is a variational method in which equilibrium is established as the minimum of a potential defined by sum of the total energy and work done by the system [4]. In the expression for system potential, a displacement function is assumed which satisfies the geometric boundary conditions of the system. The deflected needle shape is evaluated by minimizing the potential of the system. The system potential of the mechanics-based model, at any step of insertion i, is given as

$$\Pi_i = (U_{B,i} + U_{T,i}) - W_i \tag{5}$$

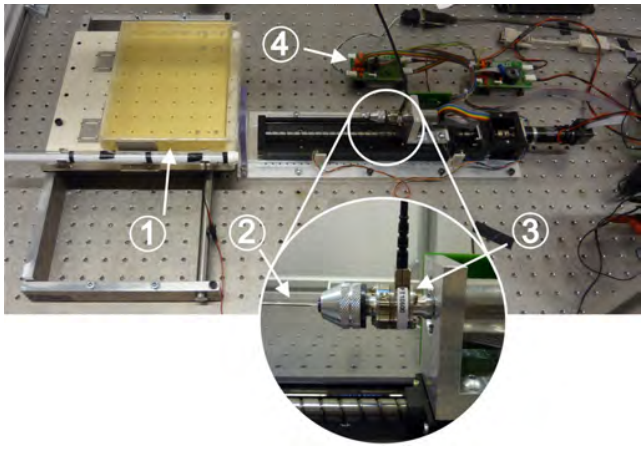

Fig. 5. Two DOF setup used for inserting needles into a phantom. ① Gelatine phantom ② Needle ③ Force/torque sensor ④ Controllers

where $U_{B,i}$ and $U_{T,i}$ are the energies associated with needle bending and the needle-tissue interaction due to tissue elasticity respectively. While W_i is the work done by transversal tip load ($F^i_{t,y}$) to deform and cut tissue at the needle tip.

B. Bending Energy

When a needle is inserted into the tissue, it bends in the transversal direction. In (5), $U_{B,i}$ is the strain energy associated with transversal needle bending. At a certain step of insertion (i) for a given needle length (L), the strain energy is given by

$$U_{B,i} = \frac{E_n I}{2} \int_0^L \left(\frac{d^2 v_i}{dx^2} \right)^2 dx_b \tag{6}$$

where v_i is the deflected needle shape, E_n the needle's Young's modulus and I is the needle's second moment of inertia.

C. Energy due to Elasticity of the Tissue

The energy due to the elastic interaction between needle and tissue is determined by the difference in deflection between the current and previous needle deflection ($v_i - v_{i-1}$) at a specified spring location (x_k which equals x_i in Fig. 4). The total energy is then defined as the sum of the energies of all the individual springs along the needle shaft

$$U_{T,i} = \sum_{k=1}^{n} \frac{1}{2} K_e \left(v_i(x_k) - v_{i-1}(x_{k-1}) \right)^2 \tag{7}$$

D. Work done by Tip Force

The work done by the transversal force $F^i_{t,y}$ during each step of insertion depends on the difference in tip deflection between the current and previous step

$$W_i = F^i_{t,y} \left(v_i(L) - v_{i-1}(L) \right) \tag{8}$$

IV. Materials and Methods

In this section the setup is presented which is used to insert needles into gelatine phantom. The needle tip tracking algorithm is also discussed here.

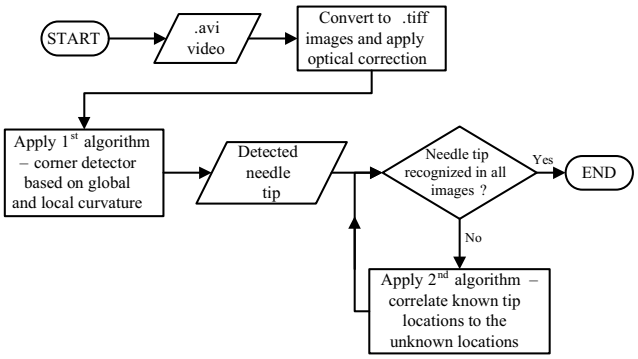

Fig. 6. Flowchart of the needle tip tracking algorithm. Input of the algorithm is a video in AVI (Audio Video Interleave) format. The tracking algorithm converts this video into series of TIFF (Tagged Image File Format) images prior to the start of the tracking procedures. This allows the needle tip to be tracked one frame at the time using the corner detector algorithm, then if necessary, by the correlation algorithm.

A. Experimental Setup

A two degree-of-freedom (DOF) needle insertion device (shown in Fig. 5) is designed for the experiments. It allows translation along and rotation about the needle's longitudinal axis. The device consists of a Misumi translation stage (type LX3010, MISUMI Group Inc. Tokyo, Japan) actuated with a Maxon Motor (type RE25, with GP26B gearhead, transmission ratio 4.4:1), and a needle rotational setup using a Maxon Motor (type ECMax22, Maxon Motor, Sachseln, Switzerland). Both motors and thus the motion are controlled using the position controller on two Elmo Whistle 2.5/60 controllers (Elmo Motion Control Ltd, Petach-Tikva, Israel). Measurement of forces/torques acting on the needle during insertion is done with a six-axis Nano17 force/torque sensor (ATI Industrial Automation, Apex, USA) located at the base of the needle. Moreover, needle insertion is recorded at 30 fps via a Sony XCD-SX90 charge-coupled device (CCD) FireWire camera (Sony Corporation, Tokyo, Japan) mounted at a height of 450 mm from the top surface of the gel. Code was written in Matlab (v7.11, Mathworks Inc., Natick, USA) to process the data retrieved from camera, Nano17 sensor and Elmo controllers.

B. Tracking of the Needle Tip

A needle tip tracking algorithm is developed based on the corner detector algorithm of Xiao et al. [15], and on the correlation algorithm of Matlab's Image Processing toolbox. The corner detector algorithm searches for the needle tip when a true corner's maximum obtuse angle is set to the needle tip bevel angle. However, due to variation in lighting intensity, it may fail to recognize the needle tip in all insertion images. Hence, the correlation algorithm is applied. It uses the knowledge of the known needle tip location and insertion speed to search for the needle tip in insertion images where the corner detector algorithm fails.

The tracking algorithm is accurate in locating the needle tip (and hence, in calculating the amount of needle tip deflection) up to 1/10 of the camera pixel resolution. The flowchart of the tracking algorithm is presented in Fig. 6.

TABLE I

PROPERTIES OF NEEDLE USED IN EXPERIMENTS AND SIMULATIONS.

Parameter	Symbol	Value
Elasticity	E_n	$200 \times 10^9\ N/m^2$
Diameter	D	$1\ mm$
Bevel angle	α	$30°$
Length	L	$130\ mm$

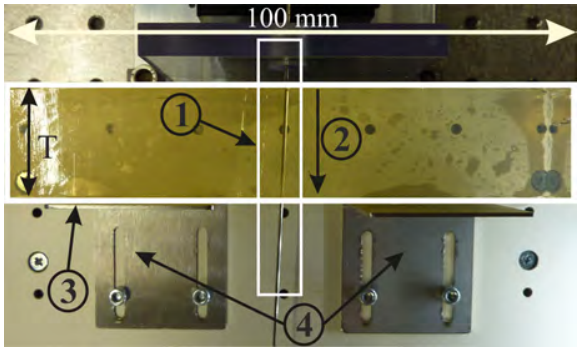

Fig. 7. Top view of the experimental setup used to measure friction force along the needle shaft. The needle ① has fully punctured a gelatine phantom. The direction of insertion is indicated by ②. A phantom ③ of 40 mm high and varying thickness T is used. ④ Two clamps were placed against the phantom to prevent it from moving during needle insertion.

V. RESULTS

Needle insertion experiments are performed using a solid, stainless steel needle with a bevel tip (Table I specifies the needle properties). Gelatine is used as a soft tissue to simulate the mechanical properties of human breast tissue [16]. The elasticity of the gelatine phantom was determined in a uniaxial compression test using the Anton Paar Physica MCR501 (Anton Paar GmbH, Graz, Austria) and was found to be 35 kPa. The needle is inserted at insertion velocities of 10 mm/s and 20 mm/s. These insertion velocities are representative insertion velocities during clinical percutaneous needle insertion procedures [17].

Experiments are performed to determine friction force along the needle shaft. The friction force and insertion force are used to calculate the horizontal tip force for a needle inserted to a pre-set insertion depth into the phantom. This tip force is then taken as input for the mechanics-based model to evaluate the needle-tissue interaction stiffness.

A. Friction

The friction along the needle shaft is determined by traversing the needle fully through a gelatine phantom (Fig. 7). As the needle tip has exited the gelatine phantom, the measured insertion force is taken as the friction force [4]. In Fig. 8 the measured insertion force during the experiment is shown for phantoms of different thickness (20, 30, 40

TABLE II

FRICTION PER UNIT NEEDLE LENGTH (f_f) EVALUATED FOR PHANTOMS OF DIFFERENT THICKNESS.

	$f_f(N/mm)$	
Phantom (mm)	10 mm/s	20 mm/s
20	0.0284	0.0329
30	0.0230	0.0322
40	0.0262	0.0344
50	0.0285	0.0359
Average	0.0265	0.0339

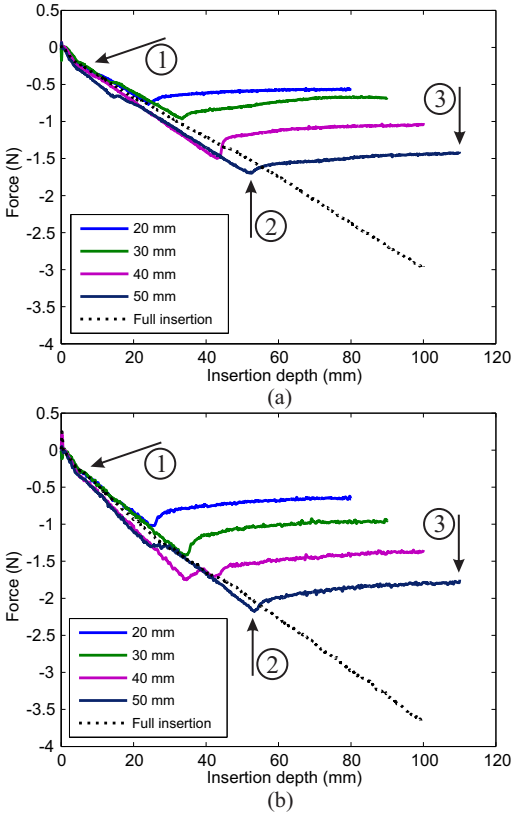

Fig. 8. Insertion force for a needle inserted through gelatine phantoms of varying thickness (20, 30, 40 and 50 mm) and for a needle inserted compeletely into a gelatine phantom (Full insertion). The experiments were performed at two different insertion velocities: (a) 10 mm/s and (b) 20 mm/s. The arrows indicate the different events during insertion for the 50 mm thick phantom: ① As the needle initially punctures the phantom, a small increase in insertion force is measured. An increase in insertion force is seen as the needle traverses through the phantom. ② The needle tip exits the tissue and this results in a drop in insertion force. ③ After the needle tip has fully traversed through the phantom, the insertion force reaches a constant value. This constant value is the horizontal friction force ($F_{f,x}$).

and 50 mm). Using (2) and the measured friction ($F_{f,x}$), the friction force per unit needle length (f_f) is calculated for each of the phantoms (Table II). Friction force is determined by taking the average friction force of the different phantoms. As expected, friction force per unit needle length is higher for insertion at 20 mm/s.

B. Needle Insertion

The needle is inserted 100 mm into the gelatine phantom. After insertion has finished, the tracking algorithm is run on the recorded video to determine the amount of needle deflection. No appreciable difference in the amount of needle deflection is observed between insertion at 10 mm/s and 20 mm/s. Therefore, only the needle deflection for the insertion performed at 10 mm/s is shown in Fig. 9(a).

Since the tracking algorithm does not give a smooth needle shape (Fig. 9(a)), a third-order polynomial (v_{pol}) is fitted to the tracked needle tip data. By taking the derivative of the polynomial to the needle's length (x_b), the slope of the needle tip is calculated

$$\theta(x_b) = \tan^{-1}\left(\frac{dv_{pol}}{dx_b}\right) \approx \frac{dv_{pol}}{dx_b} \tag{9}$$

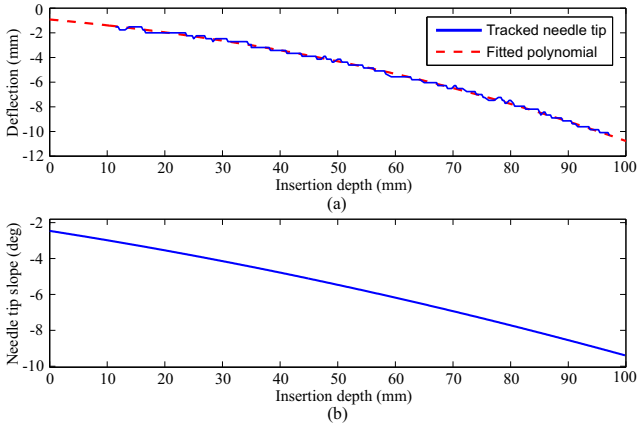

Fig. 9. (a) Shown are the tracked needle tip during insertion at 10 mm/s and a third-order polynomial (v_{pol}) fitted to this deflection data (b) Slope of the needle tip.

Using the needle tip slope (Fig. 9(b)) and the average friction per unit needle length (f_f in Table II), the horizontal component of friction ($F_{f,x}$) can be calculated for any inserted needle length (l_i)

$$F_{f,x} = \int_0^{l_i} f_f \cos\left(\theta(x_b)\right) dx_b \tag{10}$$

The horizontal tip force ($F_{t,x}$) is calculated by subtracting the calculated friction force from the insertion force (4). It can be seen (Fig. 10) that tip force is increasing in magnitude in the beginning of the insertion procedure. As insertion continues, it is expected that tip force ($F_{t,x}$) increases due to increase in needle tip slope (3) as the needle bends. However, it can be seen that tip force remains fairly constant and even decreases at some point for insertion at 20 mm/s. Air pockets in the phantom can cause these changes in the measured insertion force. Comparing the magnitude of the tip force in Fig. 10(a) with Fig. 10(b), it appears that there is no apparent difference in tip force for the 10 mm/s and 20 mm/s insertion velocities. This observation concurs with the fact that the transversal tip force causes needle bending, since there was no appreciable difference in the observed amount of deflection for insertion at 10 mm/s and 20 mm/s.

C. Simulated versus Experimental Needle Deflection

The results of the simulated needle deflection, using the mechanics-based model described in Section III, are now presented and compared with the experimental results.

In order to determine the needle shape using the Rayleigh-Ritz method, an assumed displacement function has to be defined which satisfies the geometric boundary conditions of the system. The assumed displacement function is defined by three third-order polynomials ($v_{a,i}, v_{b,i}$ and $v_{c,i}$). Each polynomial describes the deflection of the needle for a different part of the needle

$$v_i = \begin{cases} v_{a,i} & 0 \le x_b \le L/3 \\ v_{b,i} & L/3 \le x_b \le 2L/3 \\ v_{c,i} & 2L/3 \le x_b \le L \end{cases} \tag{11}$$

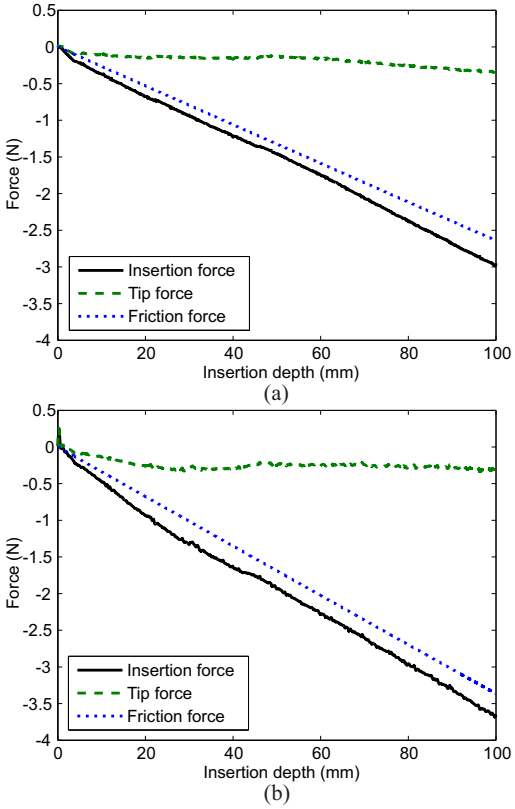

Fig. 10. The horizontal tip force ($F_{t,x}$) is calculated by subtracting the horizontal component of the friction force ($F_{f,x}$) from the insertion force (F_b) for insertion at (a) 10 mm/s and (b) 20 mm/s.

where

$$\begin{aligned} v_{a,i} &= a_{0,i} + a_{1,i}x_b + a_{2,i}{x_b}^2 + a_{3,i}{x_b}^3 \\ v_{b,i} &= b_{0,i} + b_{1,i}x_b + b_{2,i}{x_b}^2 + b_{3,i}{x_b}^3 \\ v_{c,i} &= c_{0,i} + c_{1,i}x_b + c_{2,i}{x_b}^2 + c_{3,i}{x_b}^3 \end{aligned} \tag{12}$$

The advantage of having multiple polynomials along the needle is that the actual deflection can be approximated more precisely. It is found that increasing the polynomial degree or number of polynomials beyond three did not influence needle deflection results.

The displacement function (11) should satisfy the geometric boundary conditions of the system. The needle is fixed at the base ($x_b = 0$), causing needle rotation (dv_i/dx_b) and displacement ($v_i(x_b)$) to be constrained

$$v_i(0) = \theta(0) = \frac{dv_i}{dx_b}|_{x_b=0} = 0 \tag{13}$$

The displacement function (11) also has to satisfy continuitiy conditions at the boundaries ($x_b = L/3, 2L/3$) between each of the polynomials. Applying continuity conditions for needle deflection (12) gives

$$\begin{aligned} v_{a,i}(L/3) &= v_{b,i}(L/3) \\ v_{b,i}(2L/3) &= v_{c,i}(2L/3) \end{aligned} \tag{14}$$

and applying continuity conditions for needle slope gives

$$\begin{aligned} \frac{dv_{a,i}}{dx_b} &= \frac{dv_{b,i}}{dx_b}|_{x_b=L/3} \\ \frac{dv_{b,i}}{dx_b} &= \frac{dv_{c,i}}{dx_b}|_{x_b=2L/3} \end{aligned} \tag{15}$$

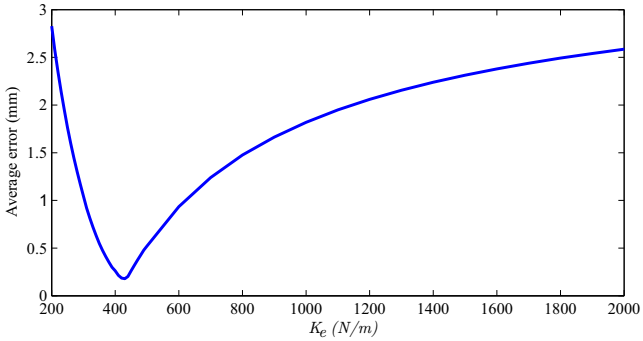

Fig. 11. Comparing the average error between simulated and experimental deflection for different values of the interaction stiffness (K_e).

Equations (13), (14) and (15) are solved for coefficients $a_{k,i}$, $b_{k,i}$ and $c_{k,i}$ for $k = 0, 1$. The remaining coefficients $a_{k,i}$, $b_{k,i}$ and $c_{k,i}$ for $k = 2, 3$ are evaluated in each step of insertion (i) by minimizing the system potential defined in (5)

$$\frac{\partial \Pi}{\partial a_{k,i}} = \frac{\partial \Pi}{\partial b_{k,i}} = \frac{\partial \Pi}{\partial c_{k,i}} = 0 \tag{16}$$

The deflected needle shape (11) is found by substituting the coefficients back into the polynomials (12).

The mechanics-based model requires the transversal tip force ($F_{t,y}$) as input in order to determine needle deflection. The transversal tip force ($F_{t,y}$) can be calculated if the tip force normal to the bevel face (F_t) is known (3). Normal tip force (F_t) can be calculated with horizontal tip force ($F_{t,x}$) and needle tip slope (θ_L)

$$F_t = \frac{F_{t,x}}{\sin(\alpha + \theta_L)} \tag{17}$$

In Fig. 10 it is shown that horizontal tip force ($F_{t,x}$) equals 0.3 N for both insertion at 10 mm/s and 20 mm/s as the needle is fully inserted. The corresponding needle tip slope (θ_L) at this point of insertion is found to be 9.2° (Fig. 9b). Using these numbers and a bevel angle (α) of 30°, a tip force of $0.47\ N$ is calculated with (17). With F_t known, transversal tip force ($F_{t,y}$) can now be calculated using needle tip slope ($\theta_{L,i}$) during insertion

$$F_{t,y} = F_t \cos(\alpha + \theta_{L,i}) \tag{18}$$

The mechanics-based model (described in Section III) is evaluated for a range of values for needle-tissue interaction stiffness (K_e). The optimal value for the interaction stiffness is found by minimizing the error between simulated and experimental deflection. The average error (in mm) is defined as the integral of the absolute error divided by the inserted needle length (l)

$$\text{average error} = \frac{1}{l}\int_{L-l}^{L} |v_{exp}(x_b) - v_{sim}(x_b)| dx_b \tag{19}$$

For low values of the interaction stiffness (K_e = 200 N/m), needle deflection is large. This results in a large error (2.7 mm) between simulation and experiment (Fig. 11). Choosing a large value ($K_e > 2000$ N/m) for the interaction stiffness results in very little needle deflection, again causing a large error. The optimal value for the interaction stiffness is

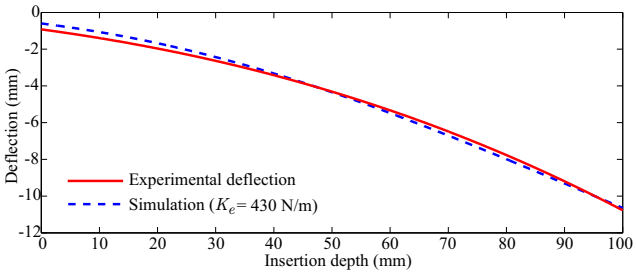

Fig. 12. Experimental needle deflection compared with simulated needle deflection using the mechanics-based model. The model was executed using the optimal stiffness value of 430 N/m.

found to be 430 N/m, the corresponding error is 0.179 mm. In Fig. 12, the simulated needle deflection is compared with the experimental needle deflection. The maximum error (0.32 mm) occurs in the beginning of the insertion (0-30 mm). A probable cause for this large error is that interaction stiffness near the edge of the phantom is different from the center. This was not taken into acount since the interaction stiffness was considered to be constant throughout the phantom.

VI. Conclusions and Future Work

In this study, needle-tissue interaction forces were identified for a bevel-tipped needle inserted into a gelatine phantom. The friction force, expressed in friction per unit needle length, was determined in a series of experiments and was found to be 0.0265 N/mm for a needle inserted at 10 mm/s and 0.0339 N/mm for a needle inserted at 20 mm/s. The tip force was extracted from the insertion force using the friction force. No appreciable difference in needle tip force was observed between a needle inserted at 10 mm/s and 20 mm/s. Using a mechanics-based model, simulated needle deflection was compared to experimental needle deflection to evaluate the needle-tissue interaction stiffness (K_e). It was found that an interaction stiffness of 430 N/m minimizes the difference between simulated and experimental needle deflection.

In this study it was assumed that the interaction stiffness is constant at each location along the needle shaft. In future work, the interaction stiffness will be considered a function of location in the phantom. Experiments were done using homogeneous gelatine phantoms. Experiments will be done using gels of varying elasticity to relate interaction stiffness to phantom imhomogeneity. The interaction stiffness of 430 N/m is related to the needle-tissue combination used in the experiments in this study. For purposes of pre-operative path planning, knowledge is required about the relationship between interaction stiffness, and needle and tissue parameters to be able to predict needle deflection. Therefore, relationships between the interaction stiffness, and constitutive needle and tissue parameters, such as tissue elasticity and needle geometry, needs to be derived. When considering future patient studies, ultrasound elastography can provide tissue elasticity such that needle deflection can be predicted using the mechanics-based model.

The mechanics-based model presented here can be used to study needle steering into soft tissue. Knowledge about the deflection is required to accurately plan the needle path, and provide appropriate control inputs to robotically steer the needle.

VII. Acknowledgements

This research (Project: MIRIAM) is funded by the Dutch Ministry of Economic Affairs and the Province of Overijssel, within the Pieken in de Delta (PIDON) initiative.

References

[1] R. J. Webster III, J. S. Kim, N. J. Cowan, G. S. Chirikjian, and A. M. Okamura, "Nonholonomic modeling of needle steering," *Int'l. J. Robotics Research*, vol. 25, no. 5-6, pp. 509–525, 2006.

[2] D. Glozman and M. Shoham, "Image-guided robotic flexible needle steering," *IEEE Transactions on Robotics*, vol. 23, no. 3, pp. 459–467, 2007.

[3] N. Abolhassani and R. V. Patel, "Deflection of a flexible needle during insertion into soft tissue," in *Proc. IEEE Int'l. Conf. Engineering in Medicine and Biology Society (EMBS)*, (New York City, USA), pp. 3858–3861, August-September 2006.

[4] S. Misra, K. B. Reed, B. W. Schafer, K. T. Ramesh, and A. M. Okamura, "Mechanics of flexible needles robotically steered through soft tissue," *Int'l. J. Robotics Research*, vol. 29, no. 13, pp. 1640–1660, 2010.

[5] N. Abolhassani, R. Patel, and M. Moallem, "Needle insertion into soft tissue: A survey," *Medical Engineering and Physics*, vol. 29, no. 4, pp. 413–431, 2007.

[6] H. Elhawary, Z. Tse, M. Rea, A. Zivanovic, B. Davies, C. Besant, N. de Souza, D. McRobbie, I. Young, and M. Lamperth, "Robotic system for transrectal biopsy of the prostate: Real-time guidance under mri," *IEEE Engineering in Medicine and Biology Magazine*, vol. 29, pp. 78–86, march-april 2010.

[7] J. J. Fütterer, S. Misra, and K. J. Macura, "Mri of the prostate: potential role of robots," *Imaging in Medicine*, vol. 2, no. 5, pp. 583–592, 2010.

[8] J. A. Engh, G. Podnar, S. Y. Khoo, and C. N. Riviere, "Flexible needle steering system for percutaneous access to deep zones of the brain," in *Proc. IEEE 32nd Annual Northeast Bioengineering Conf*, pp. 103–104, 2006.

[9] S. Misra, K. B. Reed, A. S. Douglas, K. T. Ramesh, and A. M. Okamura, "Needle-tissue interaction forces for bevel-tip steerable needles," in *Proc. IEEE Int'l. Conf. Engineering in Medicine and Biology Society (EMBS)*, (Scottsdale, AZ, USA), pp. 224–231, August 2008.

[10] R. Alterovitz, K. Goldberg, and A. M. Okamura, "Planning for steerable bevel-tip needle insertion through 2d soft tissue with obstacles," in *Proc. Int'l. Conf. Robotics and Automation (ICRA)*, (Barcelona, Spain), pp. 1640–1645, April 2005.

[11] S. Y. Ko, B. L. Davies, and F. Rodriguez y Baena, "Two-dimensional needle steering with a "programmable bevel" inspired by nature: Modeling preliminaries," in *Proc. IEEE/RSJ Int Intelligent Robots and Systems (IROS) Conf*, pp. 2319–2324, 2010.

[12] H. Kataoka, T. Washio, K. Chinzei, K. Mizuhara, C. Simone, and A. M. Okamura, "Measurement of the tip and friction force acting on a needle during penetration," in *Proc. of the 5th Int'l. Conf. on Medical Image Computing and Computer-Assisted Intervention-Part I*, MICCAI '02, (London, UK), pp. 216–223, Springer-Verlag, September 2002.

[13] A. M. Okamura, C. Simone, and M. D. O'Leary, "Force modeling for needle insertion into soft tissue," *IEEE Transactions on Biomedical Engineering*, vol. 51, no. 10, pp. 1707–1716, 2004.

[14] S. Misra, K. B. Reed, K. T. Ramesh, and A. M. Okamura, "Observations of needle-tissue interactions," in *Proc. IEEE Int'l. Conf. Engineering in Medicine and Biology Society (EMBS)*, (Minneapolis, USA), pp. 262–265, 2009.

[15] C. H. Xiao and H. Yung, "Corner detector based on global and local curvature properties," *Optical Engineering*, vol. 47, no. 5, pp. 1–12, 2008.

[16] A. Gefen and B. Dilmoney, "Mechanics of the normal woman's breast," *Technology and Health Care*, vol. 15, no. 4, pp. 259–271, 2007.

[17] N. Abolhassani, R. Patel, and M. Moallem, "Control of soft tissue deformation during robotic needle insertion," *Minimally Invasive Therapy and Allied Technologies*, vol. 15, no. 3, pp. 165–176, 2006.

Part II

'Mechanics-Based Model for Steering Flexible Needles'

Mechanics-Based Model for Steering Flexible Needles

Roy J. Roesthuis, Momen Abayazid and Sarthak Misra
MIRA – Institute for Biomedical Technology and Technical Medicine
University of Twente, The Netherlands

***Abstract*— Bevel-tipped flexible needles naturally bend when inserted into soft tissue. Steering such needles along curved paths allows one to reach locations inside the human body which are unreachable with rigid needles. In this study, a mechanics-based model is presented which predicts needle deflection during insertion into soft tissue. The model is based on a Rayleigh-Ritz formulation, and inputs to the model are forces at the needle tip and a distributed load which acts along the needle shaft. Experiments are used to evaluate these forces, and needle deflection is predicted using the model. For the *double bend* case, the model predicted the final needle tip deflection with an accuracy of 1.1 mm. The model can be extended to multiple needle rotations. For two needle rotations during insertion, the predicted error in final tip deflection is 2.4 mm. Results of this study provide insight into the mechanics of needle-tissue interaction, and can be used for robotically steering needles into soft tissue.**

I. Introduction

Percutaneous needle insertion is one of the most common minimally invasive medical procedures. It is often used to locally deliver drugs, perform biopsies or place radioactive seeds at specific locations within organs during brachytherapy. A problem with these procedures is that the intended target cannot always be reached by a straight path due to anatomical obstacles (e.g., blood vessels, nerves, bones), tissue deformation or physiological processes (e.g., respiration, fluid flow). Using thin, flexible needles with asymmetric tips, instead of the traditional rigid needles, allows the needle to bend during insertion and steer around obstacles using curved paths. Using flexible needles, the possibilities of minimally invasive are expanded since it allows to reach locations which are not reachable with rigid needles.

A number of research groups have investigated needle steering by using needles with an asymmetric (bevel) tip [1]–[7]. Needles with a bevel tip naturally bend when inserted into soft tissue due to asymmetric distribution of forces at the tip. By rotating the needle during insertion, the direction of bending is changed and this allows steering the needle (Fig. 1).

A major research objective for steering flexible needles is to have the ability to pre-operatively plan the needle path, and to intra-operatively control the needle using a robotic insertion device. Pre-operative path planning requires a model which predicts needle deflection during insertion into soft tissue. Several groups have proposed models which predict needle deflection for a bevel-tipped needle. Webster *et al.* [2] proposed a needle deflection model based on a nonholonomic kinematics approach. Their model requires experimental data fitting of model parameters for each needle-tissue combination. In humans, the needle will penetrate tissues of varying stiffness values and hence the applicability of the model is limited in biological tissue.

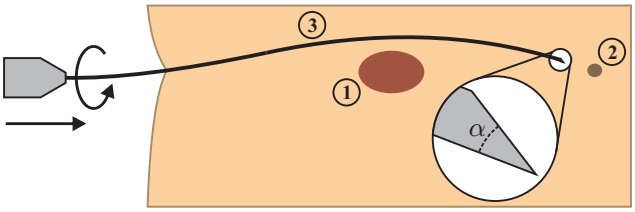

Fig. 1. A flexible needle with a bevel tip can be steered through soft tissue by performing 180° rotations during insertion. In this sketch, a flexible needle with bevel angle (α) is steered around an obstacle ①, towards a target ② by performing a rotation at ③.

A model which relates needle deflection to constitutive needle and tissue parameters such as needle geometry and tissue elasticity is better suited for biological tissues since it does not require fitting of model parameters for each needle-tissue combination. Abolhassani *et al.* [5] modeled the needle as a cantilever beam subject to a tip force. They did not investigate the relationship between needle and tissue parameters, and its effect on needle deflection. Glozman *et al.* [4] have proposed a model which uses virtual springs to predict needle deflection. The interaction between needle and tissue was modeled by distributed virtual springs along the needle shaft. They did not relate spring stiffness to tissue elasticity. Misra *et al.* [1] investigated the possibilities of a mechanics-based approach to relate needle geometric properties and tissue parameters to needle deflection. The current study expands on the work done by Misra *et al.* by proposing a modified version of their needle-tissue deflection model. The proposed model assumes that due to needle-tissue interaction, a distributed load acts along the needle shaft. Identification of the distributed load is done for two different needles and soft-tissue simulants. The model is validated using experimental data and it is shown that it can be extended to model multiple bends which is required for needle steering.

The paper is organized as follows: Section II describes the model which predicts needle deflection for a bevel-tipped needle inserted into soft tissue. In Section III, the results

This research is supported by funds from the Netherlands Organization for Scientific Research (NWO).
{r.j.roesthuis,m.abayazid,s.misra}@utwente.nl

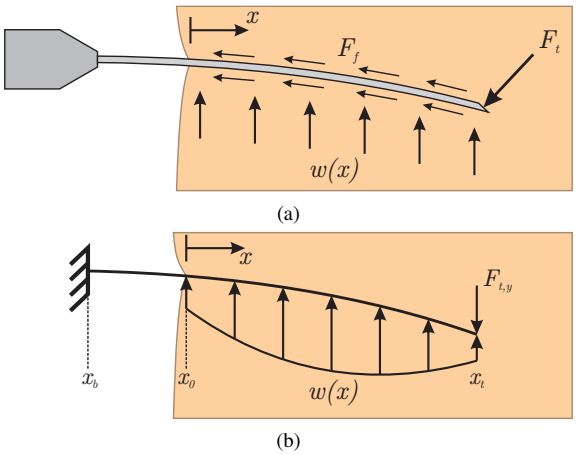

Fig. 2. (a) As a bevel-tipped, flexible needle is inserted into soft tissue it experiences friction along the needle shaft (F_f). Due to cutting of the tissue there is a tip force (F_t) that causes the needle to deflect from a straight path. The needle experiences a resistive force ($w(x)$) from the tissue as it bends. (b) The needle is modeled as a cantilever beam subject to transversal tip force ($F_{t,y}$) and distributed load ($w(x)$) which causes transversal needle bending. Assuming small needle deflections, the transversal component of friction force will be small and is therefore neglected. Needle base (x_b) and needle tip position (x_t) change as the needle is inserted into the tissue.

of needle insertion experiments are presented and compared to *single* and *double bend* simulated deflection. The paper concludes in Section IV and possible directions for future work are given.

II. Mechanics-Based Model

This section presents a mechanics-based model that predicts needle deflection for a bevel-tipped needle during insertion into soft tissue. First, a model is presented which predicts needle deflection for the case that the needle is not rotated during insertion (*single bend*). The model is then extended for the case that a single rotation is performed during insertion (*double bend*).

A. Needle Deflection Modeling

As a bevel-tipped needle is inserted into soft tissue, force is required to cut and deform tissue at the tip. Due to asymmetry of the bevel tip, the distribution of forces at the tip is also asymmetric. This is modeled by a resultant tip force (F_t) normal to the bevel face (Fig. 2a). This tip force causes the needle to deflect from a straight path.

Only transversal (y-direction) needle deflection is considered since deflection in the horizontal (x) direction is relatively small. The transversal component of the tip force ($F_{t,y}$) is considered to cause transversal needle bending (Fig. 3). The transversal tip force is related to tip force by bevel angle (α) and needle tip slope (θ_t)

$$F_{t,y} = F_t \cos(\alpha + \theta_t). \tag{1}$$

As the needle bends during insertion, it will experience a resistive force from the tissue. This resistive force is modeled as a distributed load ($w(x)$) which acts along the inserted part of the needle (Fig 2b). The profile and magnitude of the distributed load depends on needle geometrical properties and tissue elasticity.

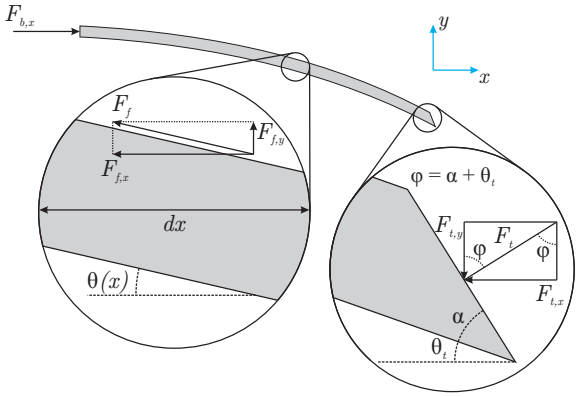

Fig. 3. The insertion force measured at the base of the needle ($F_{b,x}$) is a combination of friction force (F_f) and needle tip force (F_t). Both friction force and tip force have have horizontal (x) and transversal (y) components during insertion. The components of the friction force depend on needle slope ($\theta(x)$), and tip force components depend on needle tip slope (θ_t) and bevel angle (α).

The needle is modeled as a cantilever beam subject to needle-tissue interaction forces as it is inserted into soft tissue. The Rayleigh-Ritz method [8] is used to evaluate the deflected needle shape ($v(x)$). This is a variational method in which equilibrium is established by evaluating the minimum of a system potential (Π) defined by the sum of potential energy (U) and work done on the system (W). The system potential for a mechanical system can be written as

$$\Pi = U - W. \tag{2}$$

The Rayleigh-Ritz method requires an assumed shape (displacement) function that satisfies the geometric boundary conditions of the system [9]. For complex needle shapes, such as the double bend case, multiple shape functions need to be defined along the needle length.

B. Single Bend

When the needle is not rotated during insertion, the needle has a *single bend* shape. The model shown in Fig. 2b is used to evaluate needle deflection for the *single bend* case. The system potential for this case is written as

$$\Pi = \underbrace{U_b}_{U} - \underbrace{(W_c + W_d)}_{W}, \tag{3}$$

where U_b is the strain energy associated with transversal needle bending, W_c is the work done by transversal tip force and W_d is the work done by the distributed load. Using the Euler-Bernoulli beam theory [10], the strain energy for transversal beam bending (U_b) is calculated using

$$U_b = \frac{EI}{2} \int_{x_b}^{x_t} \left(\frac{d^2 v(x)}{dx^2} \right)^2 \mathrm{d}x, \tag{4}$$

where E (Pa) and I (m^4) are the Young's modulus and second moment of inertia of the needle, respectively.

The work done by transversal tip force ($F_{t,y}$) is given by

$$W_c = F_{t,y} v(x_t), \tag{5}$$

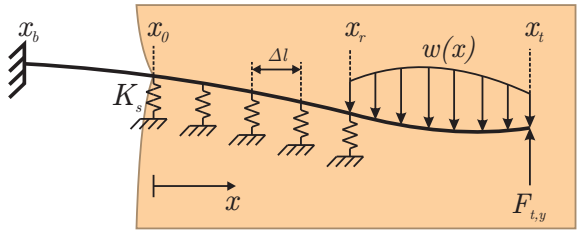

Fig. 4. For the *double bend* case, when rotation is performed at x_r, the preceding part of the needle is fixed by a series of springs. Distributed load ($w(x)$) is then applied for $x > x_r$ and tip force ($F_{t,y}$) is applied in the opposite direction due to the change of bevel tip orientation. K_s represents the individual spring stiffness.

where $v(x_t)$ is the deflection at the needle tip. The work done by the distributed load ($w(x)$) is given by

$$W_d = \int_{x_0}^{x_t} (w(x)v(x))\,\mathrm{d}x. \tag{6}$$

Needle deflection can be calculated by choosing an appropiate shape function and minimizing the system potential (3) in order to evaluate the unknown coefficients in the shape function.

C. Double Bend

Rotation of the needle during insertion results in the needle having a *double bend* shape (Fig. 4). As the needle is rotated, the orientation of the bevel tip changes and causes the needle to bend in the opposite direction. Needle deflection for *double bend* is modeled by fixing the part of the needle before rotation ($x_0 \leq x \leq x_r$) with a series of springs. This means that this part of the needle ($x_0 \leq x \leq x_r$) is resting on an elastic foundation. An elastic foundation can be approximated by a series of springs if the spacing (Δl) between the springs is sufficiently small [11]. The stiffness of the elastic foundation per unit length is given by K_0 (N/m/m). This stiffness depends on tissue elasticity, and needle and tissue geometric properties. The stiffness of the foundation (K_T) for a rotation at x_r is calculated by

$$K_T = K_0\,(x_r - x_0)\,. \tag{7}$$

For a total number of n springs, the individual spring stiffness (K_s) is calculated as

$$K_s = \frac{K_T}{n}. \tag{8}$$

Due to the elastic foundation, an additional term needs to be included in the system potential (3)

$$\Pi = \underbrace{(U_b + U_s)}_{U} - \underbrace{(W_c + W_d)}_{W}, \tag{9}$$

where U_s represents the potential energy stored in the springs

$$U_s = \sum_{i=1}^{n} \frac{1}{2} K_s v(x_i)^2, \tag{10}$$

where $v(x_i)$ is the deflection of spring i at location (x_i). Using the expression for system potential (9), the deflected needle shape is evaluated using the Rayleigh-Ritz method. Extension of the model to multiple rotations is possible by fixing the needle with a series of springs after each rotation and applying the appropriate distributed load.

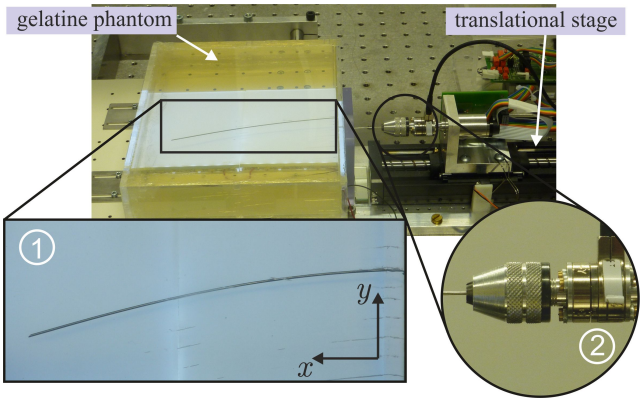

Fig. 5. Experimental setup used to insert needles into gelatine phantoms [9]. ① Topview of gelatin phantom with inserted needle. ② The load cell is mounted at the needle base.

III. Experimental Results

This section discusses the experiments performed to evaluate needle tip force and distributed load ($w(x)$) for *single* and *double bend* deflection. These are then used in the mechanics-based model to predict needle deflection.

A two degree of freedom (DOF) needle insertion device is used to insert needles into gelatin phantoms (Fig. 5). The experimental setup allows translation of the needle along and rotation about the needle's horizontal (x) axis. A 6-DOF load cell [9] (Nano17, ATI Industrial Automation, Apex, USA) is mounted at the needle base which records forces and torques during insertion. The needle tip is tracked during insertion by a Sony XCD-SX90 FireWire camera (Sony Corporation, Tokyo, Japan) mounted 450 mm above the phantom. Needle insertions are performed using Nitinol needles (E = 75 GPa) with a 30° bevel angle (α). Two different needle diameters are used: ϕ 1.0 mm and ϕ 1.5 mm. Gelatine is used a soft tissue simulant. Two gelatine phantoms with different gelatin to water ratios are used for experiments: 14.9% (gel A) and 18.0% (gel B). Increasing gelatine to water ratio results in a stiffer gel.

A. Friction and Tip Forces

The mechanics-based model requires tip force (F_t) as an input to predict needle deflection. Measuring the tip force directly during insertion is not possible since the insertion force measured at the needle base ($F_{b,x}$) is a combination of tip force and friction force (F_f). However, the horizontal component of the tip force ($F_{t,x}$) can be determined by subtracting the horizontal component of the friction force ($F_{f,x}$) from the insertion force (Fig. 3)

$$F_{t,x} = F_{b,x} - F_{f,x}. \tag{11}$$

The tip force is then calculated using needle bevel angle (α) and needle tip slope (θ_t)

$$F_t = \frac{F_{t,x}}{\sin(\alpha + \theta_t)}. \tag{12}$$

The friction force is determined using the procedure described in Fig. 6a. The insertion force during the experiments is shown in Fig. 6b for different needles (ϕ 1.0 mm and

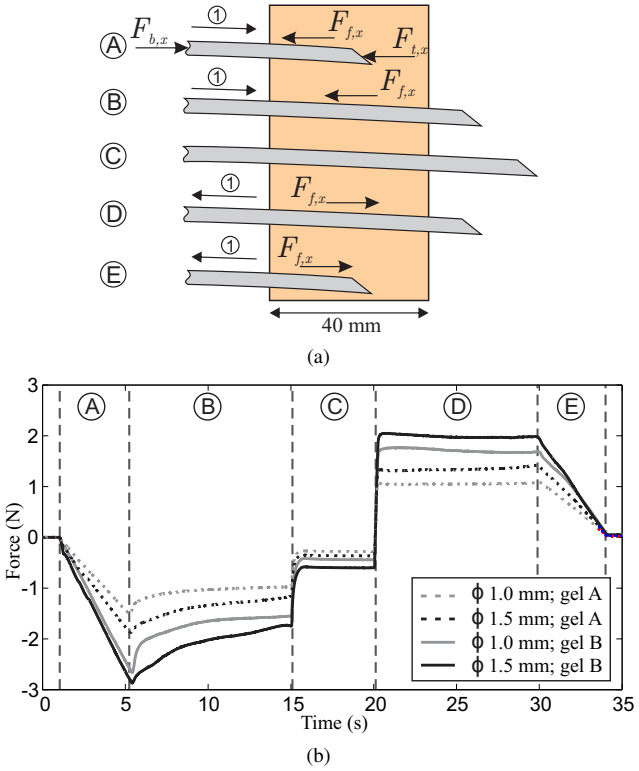

Fig. 6. (a) Calculation of friction force ($F_{f,x}$): the needle fully traverses (① indicates direction of travel) through the gelatin sample with a width of 40 mm (Ⓐ-Ⓒ). The tip force ($F_{t,x}$) acts on the needle as the tip is inside the tissue (Ⓐ). Friction force is measured during phase Ⓓ. During insertion the needle slightly bends. (b) Forces recorded at the base of the needle ($F_{b,x}$) during the different phases of the experiment for different needle-tissue combinations.

ϕ 1.5 mm) and gels (gel A and gel B). The friction force is measured during phase Ⓓ when only the needle shaft interacts with the tissue since the needle tip is outside the tissue. It can be seen in Fig. 6b that friction force increases with needle diameter and gel stiffness. As needle diameter and gel stiffness increases, the force required to push gel away during insertion also increases. This results in higher compressive forces along the needle shaft which results in an increase in friction force.

The tip force and friction force per inserted needle length (f_f) for the different needle-tissue combinations are listed in Table I. A stiffer gel results in a higher tip force since more force is required to deform the gel and cut a path. The tip force increases by 95% and 62% for ϕ 1.0 mm and the ϕ 1.5 mm diameter needles, respectively. It is also observed that tip force increases with needle diameter due to the increased surface area of the bevel face [12]. However,

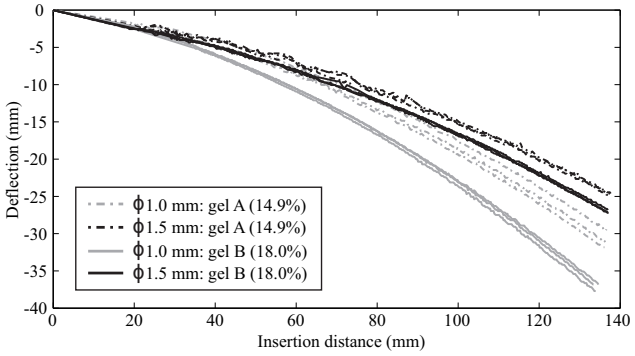

Fig. 7. Needle deflection for ϕ 1.0 and ϕ 1.5 mm diameter Nitinol needles inserted into gel A and gel B. Three insertions were performed for each experiment. The average needle tip deflection for the ϕ 1.0 mm needle is 30.8 mm (σ = 1.2 mm) for gel A and 37.1 mm (σ = 0.5 mm) for gel B. The ϕ 1.5 mm diameter needle has average tip deflection of 24.7 mm (σ = 0.1 mm) for gel A and 27.1 mm (σ = 0.2 mm) for gel B.

the increase in tip force for increased needle diameter is only minimal. An increase of 22% and 1.5% in tip force is seen for gel A and gel B, respectively.

B. Single Bend

Single bend experiments are performed using the ϕ 1.0 mm and ϕ 1.5 mm diameter Nitinol needles for gel A and gel B. The needles are inserted a distance of 140 mm in the gels at an insertion velocity of 10 mm/s. The tracked needle tip positions are shown in Fig. 7. As the needle diameter increases, the flexural rigidity of the needle increases, which implies more resistance to bending. Hence, the deflection for the ϕ 1.5 mm diameter needle is less than for the ϕ 1.0 mm diameter needle. A stiffer gel results in a higher tip force (Table I), this explains the increase in deflection for gel B compared to gel A. The variation in needle deflection (Fig. 7) is caused by out-of-plane needle deflection.

The distributed load ($w(x)$) is required to simulate *single bend* needle deflection (6). The distributed load is evaluated by fitting the model to the experimental deflection data. This fitting is done by minimizing the error (ε) between simulated needle deflection ($v_{sim}(x)$) and experimental needle deflection ($v_{exp}(x)$)

$$\varepsilon = \varepsilon_1 + \varepsilon_2, \tag{13}$$

where ε_1 is the difference in deflection along the needle shaft

$$\varepsilon_1 = \frac{1}{x_t - x_0} \int_{x_0}^{x_t} (v_{exp}(x) - v_{sim}(x))^2 \, \mathrm{d}x, \tag{14}$$

and ε_2 is the difference in deflection at the needle tip

$$\varepsilon_2 = (v_{exp}(x_t) - v_{sim}(x_t))^2. \tag{15}$$

TABLE I

FRICTION FORCE PER UNIT INSERTED NEEDLE LENGTH (f_f) AND TIP FORCE (F_t) FOR THE ϕ 1.0 MM AND ϕ 1.0 MM DIAMETER NITINOL NEEDLES. MEAN VALUES AND STANDARD DEVIATION (σ) ARE FOR FIVE EXPERIMENTS.

	f_f (N/mm)				F_t (N)			
	ϕ 1.0 mm		ϕ 1.5 mm		ϕ 1.0 mm		ϕ 1.5 mm	
Gel	mean	σ	mean	σ	mean	σ	mean	σ
A	2.63×10^{-2}	0.05×10^{-2}	3.35×10^{-2}	0.14×10^{-2}	0.73	0.11	0.89	0.05
B	4.28×10^{-2}	0.10×10^{-2}	4.97×10^{-2}	0.17×10^{-2}	1.42	0.14	1.44	0.05

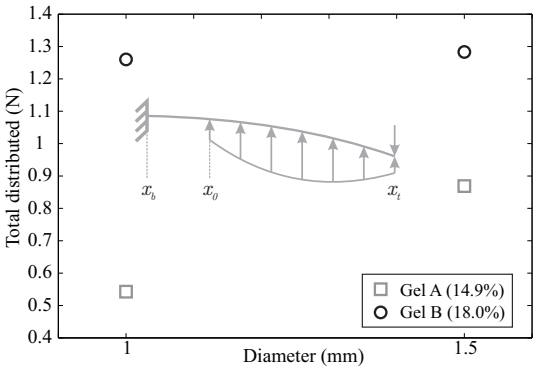

Fig. 8. Total force applied by the distributed load ($w(x)$) in the final insertion step. The force applied by the distributed load increases with needle diameter and gel stiffness.

The error (13) is minimized using MATLAB (R2010b, MathWorks Inc., Massachusetts, USA). Since the profile of the distributed load ($w(x)$) is unknown, several load profiles are evaluated (i.e., constant, linear and quadratic loads). It is found that a cubic function gives the best fit to the experimental deflection

$$w(x) = b_0 + b_1 x + b_2 x^2 + b_3 x^3. \tag{16}$$

The optimal distributed load is evaluated for each of the needles (ϕ 1.0 mm and ϕ 1.5 mm) inserted in both gels (gel A and gel B). The total force applied by the distributed load as the needle is fully inserted is shown in Fig. 8. As needle diameter and gel stiffness increase, the total force applied by the distributed load also increases due to the increase in tip force.

C. Double Bend

Double bend experiments are performed to evaluate the distributed load that needs to be applied after the needle has been rotated. Insertion experiments are performed using the ϕ 1 mm diameter needle and gel A. The needle is inserted a distance of 140 mm in the gel at an insertion velocity of 10 mm/s. Fig. 9a shows the tracked needle tip positions during the experiment for rotation at three different insertion distances: x_r = 40 mm, 70 mm and 100 mm.

As the needle is rotated, the part of the needle before rotation (i.e., $x_0 \leq x \leq x_r$) is fixed by a series of springs (Section II-C). For $x_0 \leq x \leq x_r$, the needle shaft is assumed to have relatively small displacements. This assumption is consistent with experimental observations. Hence, K_0 (7) is chosen to be 1×10^5 N/m^2. The springs are spaced 1 mm apart along the needle shaft ($x_0 \leq x \leq x_r$). Reducing the spacing between the springs does not influence the needle deflection. A total number of five shape functions along were required to accurately approximate the deflected needle shape for double bend deflection. Using more than five shape function did not influence needle deflection.

The distributed load is evaluated by minimizing the error in simulated and experimental deflection for rotations at the different insertion distances. (Fig. 9a), using the same procedure as for the *single bend* case (Section III-B). The results of the simulated deflection for the optimized load is

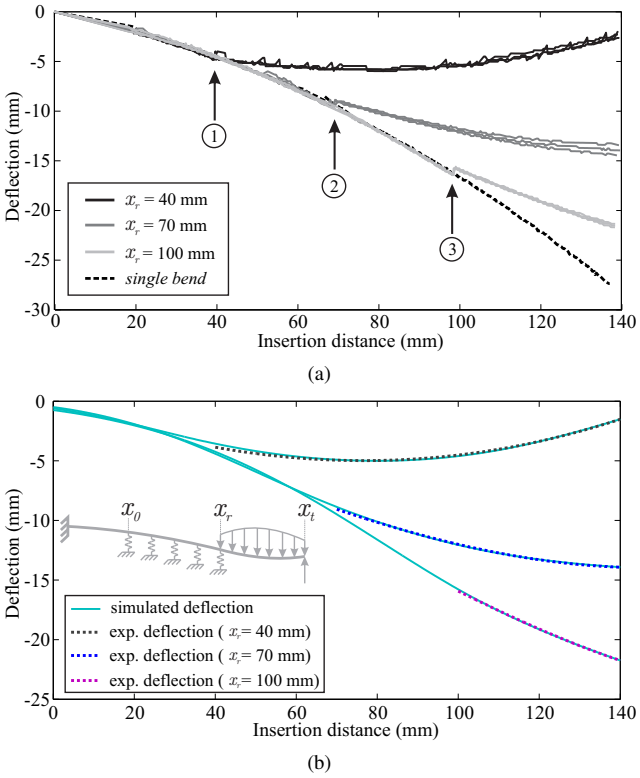

Fig. 9. (a) Needle deflection for a 1 mm diameter needle inserted in gel A. Rotation is performed at distances of 40 mm (①), 70 mm (②) and 100 mm (③). (b) Simulated needle deflection for the optimal distributed load compared with experimental deflection.

shown in Fig. 9b. It is found that the optimized loads found for rotation performed at different insertion distances shows a similar trend. This indicates that it is possible to use a single generalized distributed load for rotation at a given insertion distance. This is shown in the next section by evaluating the model for rotation at different insertion distances using the same distributed load.

D. Model Validation

The model is validated by evaluating needle deflection for a single rotation during insertion using the distributed load determined in the previous section. The ϕ 1.0 mm diameter Nitinol needle is inserted in gel A, rotation is performed at insertion distances of 55 mm and 85 mm (Fig. 10). The needles are inserted a total distance of 140 mm at an insertion velocity of 10 mm/s. Five insertions are performed for each experiment. The average error in final tip deflection between experiment and simulation for both experiments is 1.1 mm with a standard deviation (σ) of 0.6 mm.

The model is also evaluated when the needle is rotated twice during insertion. A Nitinol needle (ϕ 1.0 mm) is steered towards a target with a diameter of 3 mm (Fig.11). The needle is inserted at an velocity of 10 mm/s and needle rotations are performed at 55 mm and 100 mm in order to reach the target. The dashed line shows the evaluated needle deflection using the model. The difference in final predicted tip deflection with the experimental deflection is 2.4 mm.

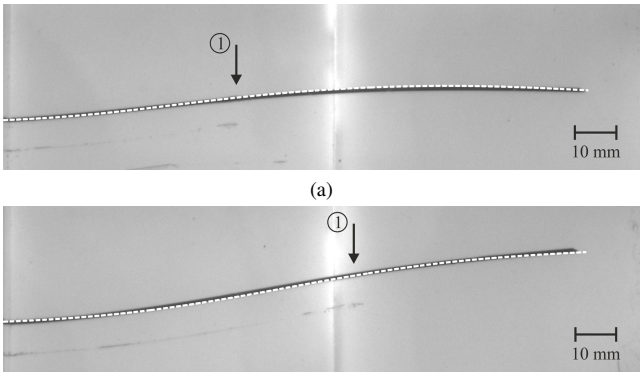

Fig. 10. *Double bend*: experimental and simulated needle deflection for a rotation (①) performed at (a) 55 mm and (b) 85 mm. The average error in final tip deflection for both experiments is 1.1 mm (σ = 0.64 mm).

IV. Conclusions and Future Work

This study presents a mechanics-based model for predicting needle deflection for steering flexible needles. The model is based on a Rayleigh-Ritz formulation where a shape function is assumed for the deflected needle. The unkown coefficients of the shape function are evaluated by minimizing the sytem potential. The system potential consists of energy terms due to needle bending and needle-tissue interaction, and work terms due to forces acting on the needle tip and along the needle shaft.

A. Conclusions

Needle insertion experiments were performed to evaluate needle tip force and distributed load for both the case where the needle is not rotated during insertion (*single bend*), and for the case of a single rotation during insertion (*double bend*). In the experiments, Nitinol needles of different diameter (ϕ 1.0 mm and ϕ 1.5 mm) were used. Gelatine phantoms with varying amount of gelatine (14.9 % and 18.0 %) were used to simulate soft tissue. It is found that both tip force and distributed load increase with needle diameter and gel stiffness. Simulation results show that needle deflection can be predicted for *double bend* deflection with an average error of 1.1 mm. It was also shown that the model can be extended predict needle deflection for multiple needle rotations.

B. Future Work

Our mechanics-based model requires needle tip force as an input to predict needle deflection. Other methods will be investigated to get a better estimate of the tip force by doing microscopic needle tip observations [12] or using a specialized experimental setup [13].

In the current study, the distributed load was evaluated for two different needles and gels. Experiments are required for different needles and soft tissue simulants to investigate the relationship between needle and tissue parameters and distributed load. This is required for predicting needle deflection when inserting needles into (inhomogeneous) biological tissue.

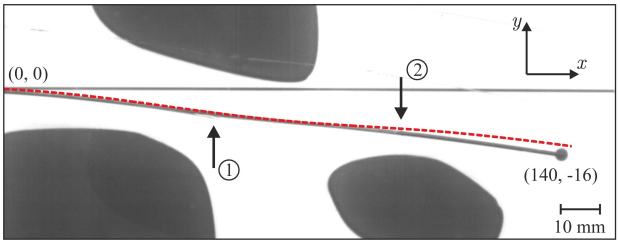

Fig. 11. A Nitinol needle (ϕ 1.0 mm) is steered towards a target (ϕ = 3 mm) by performing two rotations at insertion distances of ① 55 mm and ② 100 mm. The needle is located at an insertion distance of 140 mm and 16 mm below the needle insertion point. The dashed line is the predicted needle deflection using the model, the error in predicted tip deflection is 2.4 mm. Note: due to auto contrast of the camera, the gelatine phantom appears a lot lighter than in Fig. 10.

Our model assumes deflection in one plane (two dimensions). Predicting needle deflection for the three dimensional case requires modification of the model.

The mechanics-based model presented is shown to model multiple needle rotations during insertion and hence can be used to steer flexible needles into soft tissue. Knowledge about needle deflection is required to accurately steer needles in robot-assisted needle insertion procedures.

References

[1] S. Misra, K. B. Reed, B. W. Schafer, K. T. Ramesh, and A. M. Okamura, "Mechanics of flexible needles robotically steered through soft tissue," *Int'l. J. Robotics Research*, vol. 29, no. 13, pp. 1640–1660, 2010.

[2] R. J. Webster III, J. S. Kim, N. J. Cowan, G. S. Chirikjian, and A. M. Okamura, "Nonholonomic modeling of needle steering," *Int'l. J. Robotics Research*, vol. 25, no. 5-6, pp. 509–525, 2006.

[3] N. A. Wood, K. Shahrour, M. C. Ost, and C. N. Riviere, "Needle steering system using duty-cycled rotation for percutaneous kidney access," in *Proc. IEEE Int'l. Conf. Medicine and Biology Society (EMBC)*, pp. 5432–5435, 2010.

[4] D. Glozman and M. Shoham, "Image-guided robotic flexible needle steering," *IEEE Transactions on Robotics*, vol. 23, no. 3, pp. 459–467, 2007.

[5] N. Abolhassani and R. V. Patel, "Deflection of a flexible needle during insertion into soft tissue," in *Proc. IEEE Int'l. Conf. Engineering in Medicine and Biology Society (EMBS)*, (New York City, USA), pp. 3858–3861, 2006.

[6] N. Abolhassani, R. Patel, and M. Moallem, "Needle insertion into soft tissue: A survey," *Medical Engineering and Physics*, vol. 29, no. 4, pp. 413–431, 2007.

[7] J. A. Engh, G. Podnar, S. Y. Khoo, and C. N. Riviere, "Flexible needle steering system for percutaneous access to deep zones of the brain," in *Proc. IEEE Int'l. Conf. Annual Northeast Bioengineering Conf*, pp. 103–104, 2006.

[8] O. Bauchau and J. Craig, *Structural Analysis*. Springer, 2009.

[9] R. J. Roesthuis, Y. R. Van Veen, A. Jayha, and S. Misra, "Mechanics of needle-tissue interaction," in *Proc. IEEE Int'l. Conf. Intelligent Robots and Systems (IROS)*, September-October 2011.

[10] R. C. Hibbeler, *Mechanics of Materials*. Prentice Hall, 2008.

[11] E. S. Melerski, *Design Analysis Beams Circular Plates and Cylindrical Tanks on Elastic Foundations*. Taylor & Francis, 2000.

[12] S. Misra, K. B. Reed, B. W. Schafer, K. T. Ramesh, and A. Okamura, "Observations and models for needle-tissue interactions," in *Proc. IEEE Int'l. Conf.. Robotics and Automation (ICRA)*, (Kobe, Japan), pp. 2687–2692, May 2009.

[13] H. Kataoka, T. Washio, K. Chinzei, K. Mizuhara, C. Simone, and A. M. Okamura, "Measurement of the tip and friction force acting on a needle during penetration," in *Proc. IEEE Int'l. Conf. Medical Image Computing and Computer-Assisted Intervention (MICCAI)*, (London, UK), pp. 216–223, 2002.

Part III

‘Steering of Flexible Needles with a Bevel Tip’

Steering Flexible Needles with a Bevel Tip

Roy J. Roesthuis, Momen Abayazid and Sarthak Misra
MIRA – Institute for Biomedical Technology and Technical Medicine
University of Twente, The Netherlands

***Abstract*— Flexible needles with a asymmetric (bevel) tip naturally bend when inserted into soft tissue. These needles facilitate curved needle paths, making it possible to avoid obstacles while steering towards a desired target. A mechanics-based model is used to steer the needle towards a desired target location based on a pre-operative plan. Needle steering experiments are performed and small targeting errors of maximal 0.5 mm are achieved. Image feedback is then applied to acount for uncertainties during insertion which cause variation in needle tip deflection between different insertions. Using image feedback, the standard deviation in final needle tip deflection is reduced from 0.6 mm to 0.1 mm.**

I. Introduction

Percutaneous needle insertion is a very common minimally invasive medical procedure. As opposed to open surgery, it has the advantage of minimizing patient discomfort and results in shorter recovery times. In the procedures the needle is used to reach a specific location within the human body and to perform a specific task. In the case of brachytherapy, the needle is used to place radioactive seeds near the tumour. Another well known procedure is biospy, in which a tissue sample is taken and used for diagnosis purposes.

Needle insertion procedures are done manually by experienced physicians. Needles used in these procedures have a bevel tip to easily penetrate and cut the tissue, but this bevel tip also causes the needle to deflect from a straight insertion path. Also physiological processes such as respiration and fluid flow can cause the needle to deflect. This makes it difficult for the physician to steer the needle towards a desired location.

A number of research groups are investigating steering thin, flexible needles with a bevel tip using a robot [1]–[7]. Flexible needles allow more curved needle paths than traditional rigid, increasing the steerability of the needle. Using a robot to accurately steer the needle requires knowledge about needle deflection. Needle deflection depends on needle and tissue parameters.

In this work, a mechanics-based model is used to steer the needle towards a desired location. The mechanics-based model is compared with a kinematics-based approach presented by Webster *et al.* [2]. Two cases are considered: in the first case the models are used pre-operatively to determine the location for needle rotation in order to reach the target.

This research is supported by funds from the Netherlands Organization for Scientific Research (NWO).
{r.j.roesthuis,m.abayazid,s.misra}@utwente.nl

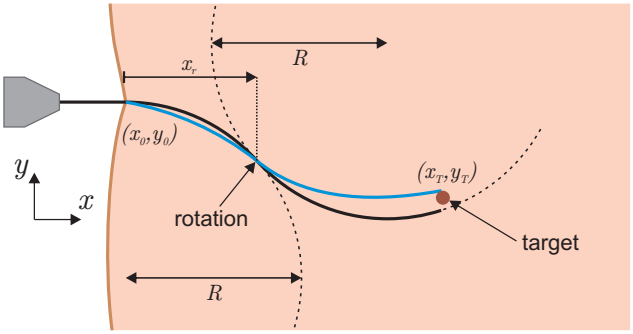

Fig. 1. Steering the needle towards a target (x_T, y_T) using the kinematics model (black) and the mechanics-based model (blue). A single rotation is performed during insertion. The kinematics model assumes that the needle tip follows a circular path (with radius R).

In the second case, image feedback of needle tip position is used to control needle rotation during insertion.

The paper is organized as follows: Section II presents two different methods for modeling needle deflection. In Section III, the method for finding needle tip position during insertion is discussed. Section IV presents the experimental results of the needle steering experiments. Finally, in Section V the conclusions of the study and future work are discussed.

II. Needle Deflection Modeling

In this section two models for predicting needle deflection are presented. The first model uses a kinematics-based approach. The second model is based on the mechanics of needle-tissue interaction to predict needle deflection.

A. Kinematics-Based Model

The idea of using nonholonomic kinematics to describe the needle path of a flexible, bevel-tipped needle has been demonstrated by Webster *et al.* [2]. Their approach assumes that the needle tip follows a circular path with constant radius of curvature. Webster *et al.* proposed using a unicycle model to describe the needle path. By having a steering constraint, the unicycle model describes a circle with constant radius of curvature (Fig. 2a). The unicycle model assumes that the needle path after rotating the needle is tangent to the needle path prior to rotation. In their experiments they observed that the needle path after rotation is not tangent to the needle path before rotation. Webster *et al.* proposed using a bicycle model to model non-tangent needle paths. The bicycle model

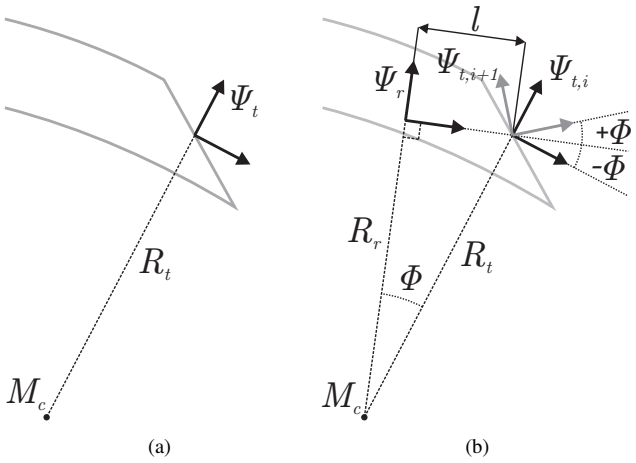

(a) (b)

Fig. 2. Using a kinematics based model, the needle path is described by a circular path with radius R_t. Two different models are shown: (a) The unicycle model assumes a frame placed at the tip of the needle which rotated around M_c. (b) The bicycle model has two wheels where the front wheel (Ψ_t) is placed at the needle tip with a fixed steering angle (Φ_t) and the rear wheel is placed a distance l behind the front wheel. When the needle is rotated, steering angle is changed from $-\Phi$ to $+\Phi$. This results a needle path which is non-tangent to the path before rotation (Fig. 3).

is shown in Fig. 2b, the model shown here differs from Webster *et al.* in the fact that the front wheel is placed at the needle tip instead of in front of the needle tip. It is found that by placing having the needle tip between the front and rear wheel, additional parameters are introduced which are unnecessary to describe the needle path.

Needle tip deflection (y_{tip}) is calculated using

$$y_{tip} = M_y + \sqrt{R_t^2 - (x_{tip} - M_x)^2}, \tag{1}$$

where (M_x, M_y) and R_t represent the coordinates of the centre and the radius of the circle desribing the current needle path. After needle rotation, the needle path is described using a new circle. The coordinates of this circle centre $(M_{x,i+1}, M_{y,i+1})$ depend on the coordinates of the previous circle $(M_{x,i}, M_{y,i})$ and the moment of rotation indicated by the angle (θ). For the unicycle model the circle centre is calculated by

$$\begin{aligned} M^{uni}_{x,i+1} &= R_t \cos(\theta) + x_{r,i}, \\ M^{uni}_{y,i+1} &= R_t \sin(\theta) + y_{r,i}. \end{aligned} \tag{2}$$

For the bicycle model, changing the steering angle from $-\Phi$ to $+\Phi$ results in a different circle centre

$$\begin{aligned} M^{bic}_{x,i+1} &= R_t \cos(\theta + 2\Phi) + x_{r,i}, \\ M^{bic}_{y,i+1} &= R_t \sin(\theta + 2\Phi) + y_{r,i}. \end{aligned} \tag{3}$$

The needle path is now described using (1). When a rotation is performed, the centre of the circle desribing the needle path after rotation is calculated using (2) or (3), depending on the model of choice.

B. Mechanics-Based Model

Since the paper is still in preparation, the reader is referred to Part II of this thesis (Section II. Mechanics-Based Model) for the mechanics-based model.

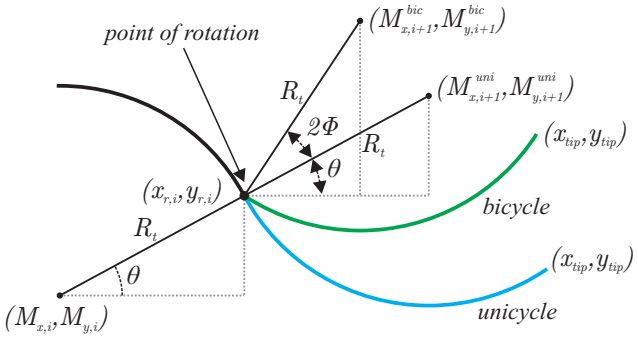

Fig. 3. The kinematics model assumes a circular needle path with radius R_t. Before rotation, the needle tip rotates around a circle with coordinates $(M_{x,i},\ M_{y,i})$. The unicycle model assumes that the circle after rotation (blue) is tangent to the path prior to rotation. The needle tip then rotates around the circle centre $(M^{uni}_{x,i},\ M^{uni}_{y,i})$. Using the bicycle model, the midpoint $(M^{uni}_{x,i+1},\ M^{uni}_{y,i+1})$ is rotated an angle of twice the steering angle (2Φ) around the rotation location $(x_{r,i}, y_{r,i})$ resulting in the green needle path with midpoint $(M^{bic}_{x,i+1},\ M^{bic}_{y,i+1})$.

III. Image Processing

Needle tip tracking during insertion is done using subtraction of subsequent frames as demonstrated by Abayazid *et al* [8]. I refer the reader to Appendix A of this thesis for more information about this subtraction technique.

IV. Experimental Results

In this section, experiments are performed in which the needle is steered towards a desired target location (Fig. 1). Two different cases of needle steering are investigated. In case I, the needle is steered towards the target using a single rotation during insertion. The location of rotation is determined by the mechanics-based model and compared with the kinematic unicycle and bicycle models. In case II, the mechanics-based model is used as a pre-operative planner to determine the location for an initial location. After the initial rotation, the kinematic bicycle model is used to control needle rotation during insertion using image feedback.

A. Materials and Methods

In the experiments a 0.8 mm diameter Nitinol needle with a 30° bevel tip is used. The needles are inserted with a speed of 10 mm/s. Gelatin is used as soft tissue simulant. Gelatin phantoms (200×170×30 mm) are made by mixing 14.9% (by-weight-ratio) gelatin with water. The Young's modulus of the gelatine phantom is determined in a uni-axial compression test using the Anton Paar Physica MCR501 (Anton Paar GmbH, Graz, Austria) and is found to be 35 kPa. This value is within the range that is found in human breasts [9]. The needles are inserted using a 2 degree of freedom (DOF) robotic setup [10] which allows translation of the needle in the insertion direction and rotation about the needle's longitudinal (x-axis). Videos of the experiments are recorded by a camera (Sony XCD-SX90, Sony Corporation, Tokyo, Japan) which is mounted 450 mm above the setup.

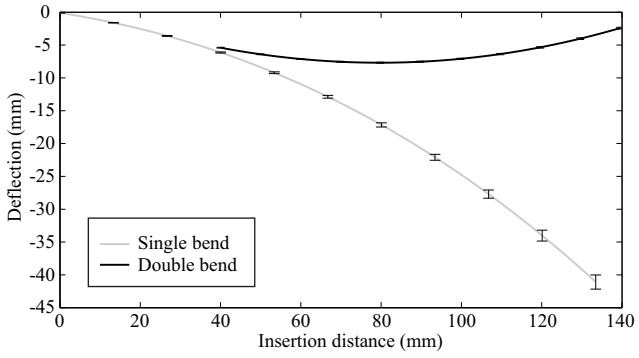

Fig. 4. Experimental deflection for a single and double bend (x_r = 40 mm) experiment. The solid lines show the average tip deflection, and the errorbars represent the standard deviation. Average final tip deflection is -2.4 mm (σ = 0.1 mm) and -41.1 mm (σ = 1.1 mm) for double bend and single bend, respectively.

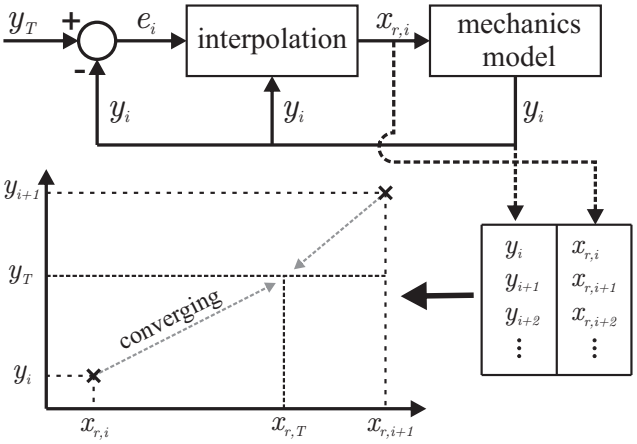

Fig. 5. Interpolation is used to determine the rotation distance ($x_{r,T}$) to steer the needle towards the desired target deflection (y_T). The interpolation table is updated after each iteration, causing the error (e_i) to decrease and the rotation location to converge to the solution.

The needle tip location is determined using the recorded videos and a corner detection algorithm [10].

B. Model Fitting

The distributed load for the needle-tissue combination used in this experiment needs to be evaluated for the mechanics-based model. Experimental results are also required to evaluate parameters (R_t and Φ) of the kinematic model. Therefore, a series of single and double bend experiments are performed. For each insertion, the needle is positioned to a new location. A total of 9 insertions were done for the single bend experiment and 8 insertions for the double bend experiment. For the single bend, the needle is inserted a distance of 140 mm inside the gelatin phantom. In the double bend experiments, the needle is inserted 40 mm, then rotated 180°, and further inserted to a total distance of 140 mm. The tip deflection during insertion for the double and single bend are shown in Fig. 4. The deviation in deflection for the single bend experiment is caused by differences in initial positioning of the needle tip between insertions.

The kinematics model assumes that the needle tip follows a circular path. The radius of curvature of the needle path is determined by fitting a circle to the (single bend) experimental deflection using a method described by Pratt *et al.* [11]. The average radius of curvature was determined to be 332.4 mm (Table I). The steering angle (Φ) for the bicycle model is calculated by substituting the experimental deflection in the equations describing the needle path(eqs. (1) to (3)) and then solve for the steering angle. A steering angle of 2.68° is found for this needle-tissue combination.

In contrast to previous work [10], here a constant tip force (F_t) is assumed. This allows faster evaluation of the model since tip force does not need to be recalculated during insertion. In the previous work, tip forces were determined for the same Nitinol needles with a diameter of 1.0 mm. Tip forces for these needles were in the range of 0.4 N. Since it is assumed that tip force is proportional to the area of the bevel face [1], decreasing needle diameter from 1.0 mm to 0.8 mm would result in a decrease of tip force from 0.4 N to approximately 0.25 N.

Using the constant tip force, the distributed load is evaluated for both the single and double bend case at discrete insertion step intervals of 1 mm by fitting the simulated deflection (v_{exp}) to the experimental deflection (v_{exp}). To fit the model to the experimental data, the following error function is used

$$\varepsilon = \varepsilon_1 + \varepsilon_2, \tag{4}$$

where ε_1 is the difference in deflection along the needle shaft

$$\varepsilon_1 = \frac{1}{x_t - x_0} \int_{x_0}^{x_t} (v_{exp}(x) - v_{sim}(x))^2 \, \mathrm{d}x, \tag{5}$$

and ε_2 is the difference in deflection at the needle tip

$$\varepsilon_2 = (v_{exp}(x_t) - v_{sim}(x_t))^2. \tag{6}$$

A polynomial expression for the distributed load was found to give a good fit to the experimental deflection

$$w(x) = a_0 + a_1 x + a_2 x^2 + a_3 x^3. \tag{7}$$

The coefficients ($a_0 ... a_3$) are calculated by minimizing (4).

C. Case I: Single Rotation Needle Steering

The goal is to steer the needle towards a target located at (x_T, y_T) with initial coordinates (x_0, y_0) by rotating the needle once during insertion (Fig. 1). The mechanics-based

TABLE I

RESULTS OF FITTING CIRCLES TO NEEDLE TIP DEFLECTION OF SINGLE BEND EXPERIMENTS (9 EXPERIMENTS, STANDARD DEVIATION GIVEN BY σ). THE CIRCLE CENTRE COORDINATES IS GIVEN BY (M_x,M_y) AND THE CIRCLE RADIUS IS GIVEN BY R_t.

	M_x (mm)	M_y (mm)	R_t (mm)
Mean	-28.3	-331.4	332.4
σ	1.84	13.3	13.4

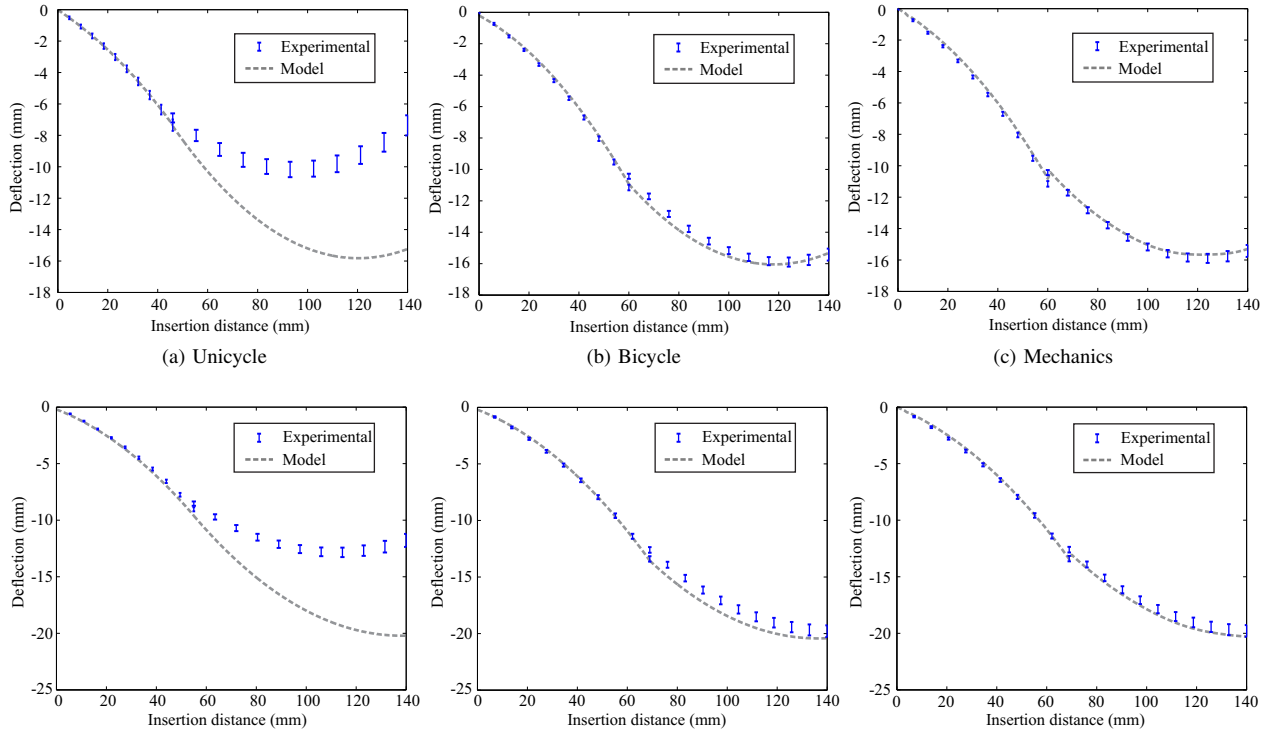

(a) Unicycle (b) Bicycle (c) Mechanics

(d) Unicycle (e) Bicycle (f) Mechanics

Fig. 6. Different models have been used to steer the needle towards two different target locations: (a)-(c) y_T = -15.3 mm, (d)-(f) y_T = -20.3 mm. For each experiment a total of 5 insertions were performed. Results of the experiments shown here are given in Table II.

model and the kinematics model are used to determine at which distance (x_r) the needle should be rotated. Two experiments are performed with targets at equal insertion distances of 140 mm ($x_{T,1}$ = $x_{T,2}$ = 140 mm) but with different deflections of -15 mm ($y_{T,1}$) and -20 mm ($y_{T,2}$).

For the case of a single rotation, for increasing rotation distance, the final tip (y_T) deflection also increases. This relationship is however not linear. To find the rotation distance using the mechanics-based model, interpolation is used (Fig. 5). Initially, the interpolation table contains entries for no rotation, and rotation at a small rotation distance of 40 mm. After each iteration, the interpolation table is updated. When the resulting error (e_i) between predicted and desired final tip deflection does not further decrease, the rotation distance is found. Since distributed load is evaluated for discrete intervals of 1 mm, needle tip deflection can only be evaluated for 1 mm intervals. For the target at -15 mm, a rotation distance of 60 mm was found after 4 iterations of the model, resulting in a predicted deflection of -15.3 mm. A rotation distance of 69 mm was found for the target at -20 mm after 4 iterations, resulting in a predicted deflection of -20.3 mm.

The rotation distance for the kinematics unicycle and bicycle model is determined by solving the equations describing the needle path (eqs. (1) to (3)) for the final tip position. To compare with the mechanics model, the desired deflection for the targets is also set at -15.3 mm and -20.3 mm. Using the unicycle model, rotation distances are calculated to be 46 mm ($y_T = -15.3$ mm) and 55 mm ($y_T = -20.3$ mm). The bicycle model gives almost the same rotation distances as the mechanics-based model: 60 mm ($y_T = -15.3$ mm) and 68.8 mm ($y_T = -20.3$ mm).

TABLE II

RESULTS OF STEERING THE NEEDLE TOWARDS A TARGET AT TWO DIFFERENT LOCATIONS (y_T) USING THREE DIFFERENT MODELS. NOTE, ROTATION DISTANCE (x_r), EXPERIMENTAL TIP DEFLECTION ($y_{T,exp}$), TARGETING ERROR ($e(x_T)$), MAXIMUM ERROR (e_{max}) AND THE STANDARD DEVIATION OF FINAL TIP DEFLECTION ($\sigma(x_T)$).

Model	y_T (mm)	x_r (mm)	$y_{T,exp}$ (mm)	$e(x_T)$ (mm)	e_{max} (mm)	$\sigma(x_T)$ (mm)
Unicycle	-15.3	46	-7.4	7.9	7.9	0.6
	-20.3	55	-11.8	8.5	8.5	0.6
Bicycle	-15.3	60	-15.4	0.1	0.5	0.4
	-20.3	69	-19.8	0.5	1.1	0.5
Mechanics	-15.3	60	-15.4	0.1	0.3	0.4
	-20.3	69	-19.8	0.5	0.6	0.5

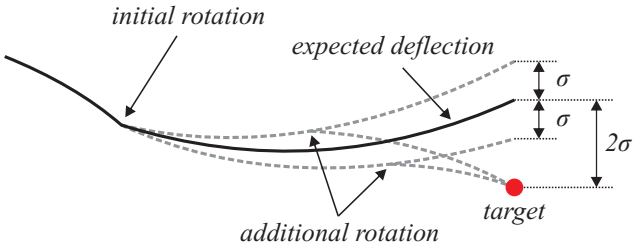

Fig. 7. An initial rotation is performed such that the target is expected to be missed by two times the standard deviation (2σ). The target can still be reached by performing additional rotations after the initial rotation.

Insertion experiments are performed in which the needle is rotated at the rotation distances as determined using the different models. The resulting needle tip deflection for the experiments are shown in Fig. 6 and in Table II. The unicycle model results in large targeting errors of 7.9 mm and 8.5 mm for the target at -15.3 mm and -20.3 mm respectively. The bicycle and mechanics-based model give the same results in targeting error. The maximum error in tip deflection is smaller for the mechanics-based model: 0.3 mm and 0.6 mm for the mechanics-based model and 0.5 mm and 1.1 mm for the bicycle model.

Despite the fact that targeting error is small in the experiments using the pre-operative plan, the target can still be missed due to the variation in deflection between different insertions. In the next paragraph, image feedback is used to account for this.

D. Case II: Needle steering with Image Feedback

Uncertainties during needle insertion cause variation in needle tip deflection between insertions. This can cause the needle to miss the target when needle is steered based on the pre-operative plan alone. By providing image feedback of needle tip position during insertion, it is possible to correct for errors in the expected deflection by controlling needle rotation during insertion.

During insertion, needle tip position is acquired as described in Section III. An pre-operative plan is made based on the location of the target using the mechanics-based model. This means that the location for an initial rotation is determined. This location is chosen such that the variation in final needle tip position is taken into account (Fig. 7). After the initial rotation, the bicycle model is used in combination with image feedback to intra-operatively steer the needle towards the target. Using image processing, needle tip angle is calculated during insertion and this is used to calculated the circle centre. This circle centre is used to determine when the next needle rotation is to be performed.

Two experiments are peformed with targets at -15.5 mm (experiment II.A) and -20.7 mm (experiment II.B). Assuming a standard deviation of 1 mm, the location of the initial rotation is determined such that the needle tip is expected to deflect to -13.5 mm and -18.7 mm for experiment II.A and II.B (Fig. 7), respectively. Using the mechanics-based model, this results in initial rotation locations of 60 mm for II.A and 71 mm for II.B. Five insertions are done for both experiments. On average, the number of rotations performed after the initial rotation was 2. The resulting needle tip deflection is shown in Fig.8 and targeting error is shown in Table III. The targeting error is not considerably smaller than the targeting error observed in case I (Table II). However, final tip deflection is almost equal for all insertions, indicating that the targeting error is most likely caused by a systematic error.

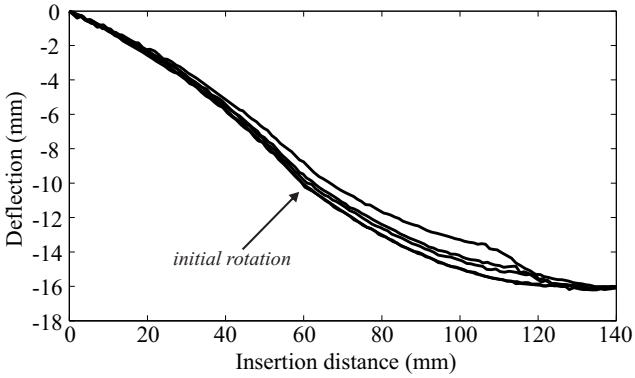

(a)

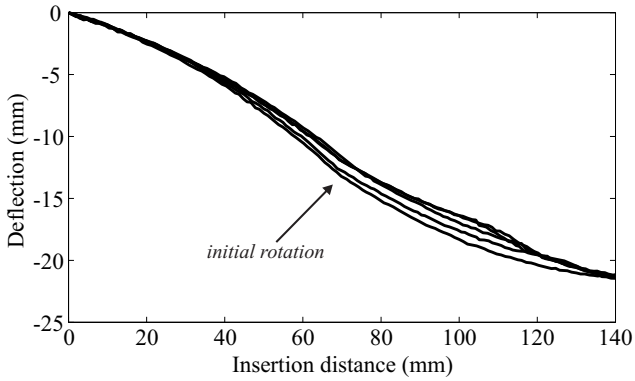

(b)

Fig. 8. Using image feedback, needle rotation is controlled during insertion. This enables steering the needle accurately towards the target for each insertion. Five insertions are performed for both experiments. (a) y_T = -15.5 mm and (b) y_T = -20.7 mm.

V. Conclusions and Future Work

In this work a mechanics-based model is used for steering flexible needles. Experiments are performed using a 0.8 mm diameter Nitinol needle with a bevel tip. Two different

TABLE III

Results of steering the needle using image feedback. Note, target deflection (y_T), experimental tip deflection ($y_{T,exp}$), targeting error ($e(x_T)$), standard deviation of final tip deflection ($\sigma(x_T)$) and the average number of rotations (n_{rot}) after the initial rotation.

Exp	y_T (mm)	$y_{T,exp}$ (mm)	$e(x_T)$ (mm)	$\sigma(x_T)$ (mm)	n_{rot}
II.A	-15.5	-16.0	0.5	0.05	2
II.B	-20.7	-21.3	0.6	0.14	2

cases were evaluated: in the first case, a needle was steered towards a desired location by perfoming a single rotation during insertion. Different models were used to determine the location of rotation: unicycle model, bicycle model and the mechanics-based model. The bicycle and mechanics-based model gave equal results in targeting error: 0.1 mm for the target at -15.3 mm and 0.5 mm for the target at -20.3 mm. However, the maximum error for the mechanics-based model was smaller than the bicycle model. It was observed that there is variation in needle tip deflection between insertions for the same experiment. This can cause the needle to miss the target when steering is done using only the pre-operative plan.

In the second case image feedback of needle tip position is used to control needle rotation intra-operatively. This resulted in a reduction of the standard deviation in final needle tip deflection from about 0.5 mm to 0.1 mm. This shows that accurate needle steering is possible using image feedback.

In the experiments performed in this study, obstacles were not considered. In future work, obstacles will be considered and this requires path planning procedures in order to avoid the obstacles.

All the experiments were done using homogoneous gelatine phantoms. Experiments will be performed using inhomogeneous (biological) tissue in future work.

For such tissues, more research is required regarding the mechanics-based model. The relationship between distributed load and tissue elasticity needs to be investigated. Ultrasound elastography can then be used to visualize the distribution of stiffness within such tissues, and provide inputs to the mechanics-based model to predict needle deflection. The mechanics-based model can then be used to pre-operatively plan a path. When it is possible to run the mechanics-based model in real time, the mechanics-based model can also be used for intra-operative control.

REFERENCES

[1] S. Misra, K. B. Reed, B. W. Schafer, K. T. Ramesh, and A. M. Okamura, "Mechanics of flexible needles robotically steered through soft tissue," *Int'l. J. Robotics Research*, vol. 29, no. 13, pp. 1640–1660, 2010.

[2] R. J. Webster III, J. S. Kim, N. J. Cowan, G. S. Chirikjian, and A. M. Okamura, "Nonholonomic modeling of needle steering," *Int'l. J. Robotics Research*, vol. 25, no. 5-6, pp. 509–525, 2006.

[3] N. A. Wood, K. Shahrour, M. C. Ost, and C. N. Riviere, "Needle steering system using duty-cycled rotation for percutaneous kidney access," in *Proc. IEEE Int'l. Conf. Medicine and Biology Society (EMBC)*, pp. 5432–5435, 2010.

[4] D. Glozman and M. Shoham, "Image-guided robotic flexible needle steering," *IEEE Transactions on Robotics*, vol. 23, no. 3, pp. 459–467, 2007.

[5] N. Abolhassani and R. V. Patel, "Deflection of a flexible needle during insertion into soft tissue," in *Proc. IEEE Int'l. Conf. Engineering in Medicine and Biology Society (EMBS)*, (New York City, USA), pp. 3858–3861, 2006.

[6] N. Abolhassani, R. Patel, and M. Moallem, "Needle insertion into soft tissue: A survey," *Medical Engineering and Physics*, vol. 29, no. 4, pp. 413–431, 2007.

[7] J. A. Engh, G. Podnar, S. Y. Khoo, and C. N. Riviere, "Flexible needle steering system for percutaneous access to deep zones of the brain," in *Proc. IEEE Int'l. Conf. Annual Northeast Bioengineering Conf*, pp. 103–104, 2006.

[8] M. Abayazid, R. Reilink, and S. Misra, "Image-guided flexible needle steering," in *Proc. Int'l. Conf. Robotics and Automation (ICRA)*, (St. Paul, USA), May 2012. Under Review.

[9] A. Gefen and B. Dilmoney, "Mechanics of the normal woman's breast," *Technology and Health Care*, vol. 15, no. 4, pp. 259–271, 2007.

[10] R. J. Roesthuis, Y. R. Van Veen, A. Jayha, and S. Misra, "Mechanics of needle-tissue interaction," in *Proc. IEEE Int'l. Conf. Intelligent Robots and Systems (IROS)*, September-October 2011.

[11] V. Pratt, "Direct least-squares fitting of algebraic surfaces.," *Computer Graphics (ACM)*, vol. 21, no. 4, pp. 145–152, 1987.

Conclusions and Future Work

In this study we have derived a mechanics-based model for predicting deflection of flexible needles with an asymmetric needle tip inserted into soft tissue. This model is based on the interaction between needle and tissue. Experiments have been done using both steel needles and flexible Nitinol needles, gelatine phantoms were used as soft tissue simulants. Needle-tissue interaction forces have been identified and measured. Needle tip force was used to model needle deflection for the single bend case, when no rotation is performed.

The mechanics-based model was modified to predict needle deflection for the case in which the the needle is rotated during insertion (double bend). It has been shown that we are able to predict deflection for the double bend case (1.0 mm diameter Nitinol needle) with an accuracy of 1.1 mm.

Finally, we have shown that we were able to steer a 0.8 mm diameter Nitinol needle with a bevel tip towards a desired location, using the mechanics-based model. A comparison was made with the kinematics-based kinematic bicycle model. Targeting error using the mechanics-, and kinematics-based model in these experiments was found to be equal, giving an error of 0.6 mm. The maximum observed error during insertion was found to smaller using the mechanics-based model: 0.6 mm compared to 1.1 mm using the bicycle model.

Uncertainties during insertion can cause variation in needle deflection between insertions and the target can still be missed. Therefore we have used image feedback in order to control needle rotation during insertion. An initial rotation was made, based on a pre-operative plan using the mechanics-based model. After this initial rotation, needle rotation was controlled using image feedback and the kinematics-based bicycle model. We have shown that using image feedback, standard deviation of final needle tip position was decreased from 0.6 mm to 0.1 mm. Targeting error did not decrease, but this was due to a systematic error in the control algorithm.

The mechanics-based model provides a basis for further research into needle steering when inhomogeneous (biological) tissues are considered. However showing similar results with the kinematic bicycle model in the experiments done in this study, it is believed that the mechanics-based model will be more accurate in future studies with real biological tissue.

Future Work

The proposed model provides a basis for further research into flexible needle steering. However, more research is required to investigate, and better understand the relationship between distributed load and needle and tissue parameters. If this relationship is fully understood, it is possible to plan paths for more complex and inhomogeneous tissues which include anatomical obstacles. Ultrasound elastography can then be employed to determine the stiffness distribution inside a certain tissue. This can than be provided as an input for the mechanics-based model which will then take care of planning a pre-operative path.

Needle deflection is relatively small for the experiments performed in this study. If large needle deflections are considered, the mechanics-based model needs to be extended since it does not take into account the horizontal deflection which cannot be ignored for large deflections.

Evaluation of the model in real time is required to be able to use it for intra-operative control. When looking at medical procedures, planning a needle path is a three dimensional problem. These requirements need modifications of the current model and this will be done in future work.

Appendix A

Real time needle tracking is needed for steering the needle tip to reach the target. The position of the needle tip is determined using subtraction technique. First, the captured frame is converted to a binary image by selecting a threshold and then the image is inverted. The same process is applied on each captured frame. The pixel values of two successive frames after inverting the pixel values are subtracted. The resultant image will show a bright area which represents the increase of the needle length. The needle tip position is determined by calculating the centroid of the resultant image which is assumed to be the location of the needle tip in the last frame (Fig. 3). The centroid calculations are based on image moments. The image moments M_{ij} of the resultant image after the subtraction of the two frames are defined as

$$M_{ij} := \sum_x \sum_y x^i y^j I(x, y), \tag{1}$$

where $I(x, y)$ is the pixel value in the position (x,y) in the image, and x and y range over the search window. i and j are the order of moment in the direction of x and y, respectively. The x- and y-coordinate of the image centroid is X_{cen} and Y_{cen}, respectively, and calculated as

$$X_{cen} = \frac{M_{10}}{M_{00}} \tag{2}$$

$$Y_{cen} = \frac{M_{01}}{M_{00}} \tag{3}$$

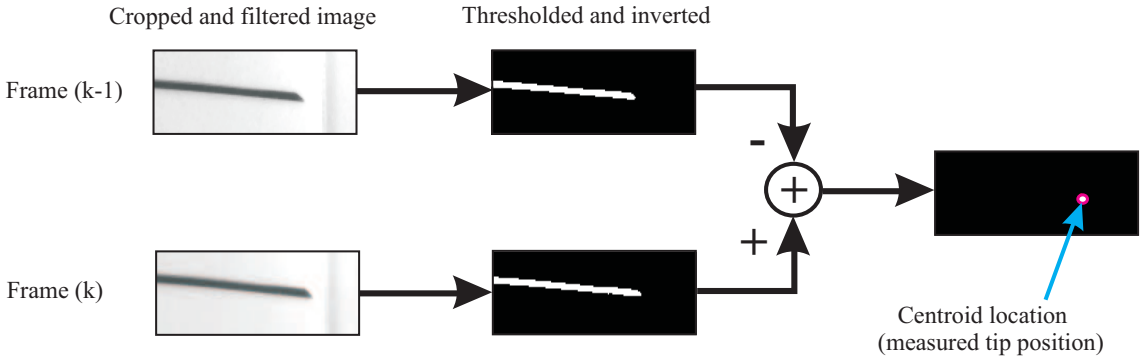

Figure 3: Schematic of the needle tip tracking algorithm. Frame (k) of the image is cropped to get the region of interest and then thresholding is applied to get a binary (black and white) image. The same process is applied on frame (k-1), and then frame (k-1) is subtracted from frame (k) to get the increase in the needle length in the image. The centroid of the image is calculated to determine the location of the needle tip in the image.